UNIVERSITÉ TOULOUSE III – PAUL SABATIER
FACULTÉS DE MÉDECINE

ANNÉE 2022 2022 TOU3 1583

THÈSE

POUR LE DIPLÔME D'ÉTAT DE DOCTEUR EN MÉDECINE

MÉDECINE SPÉCIALISÉE CLINIQUE

Présentée et soutenue publiquement

par

Emma BIQUET

le 09/09/2022

LUNG ULTRASOUND PIXEL-LEVEL COMPUTER-ASSISTED ANALYSIS FOR COVID-19 PATIENTS

Directeur de thèse : Dr Amazigh AGUERSIF

JURY

Monsieur le Professeur Stein SILVA	Président
Madame le Docteur Fanny BOUNES	Assesseur
Madame le Docteur Béatrice RIU	Assesseur
Monsieur le Docteur Clément DELMAS	Assesseur
Madame le Docteur Caroline BIENDEL	Suppléant
Monsieur le Docteur Amazigh AGUERSIF	Suppléant

FACULTE DE SANTE
Département Médecine Maieutique et Paramédicaux
Tableau des personnels HU de médecine
Mars 2022

Professeurs Honoraires

Doyen Honoraire	M. CHAP Hugues
Doyen Honoraire	M. GUIRAUD-CHAUMEIL Bernard
Doyen Honoraire	M. LAZORTHES Yves
Doyen Honoraire	M. PUEL Pierre
Doyen Honoraire	M. ROUGE Daniel
Doyen Honoraire	M. VINEL Jean-Pierre
Professeur Honoraire	M. ABBAL Michel
Professeur Honoraire	M. ADER Jean-Louis
Professeur Honoraire	M. ADOUE Daniel
Professeur Honoraire	M. ARBUS Louis
Professeur Honoraire	M. ARLET Philippe
Professeur Honoraire	M. ARLET-SUAU Elisabeth
Professeur Honoraire	M. ARNE Jean-Louis
Professeur Honoraire	M. BARRET André
Professeur Honoraire	M. BARTHE Philippe
Professeur Honoraire	M. BAYARD Francis
Professeur Honoraire	M. BLANCHER Antoine
Professeur Honoraire	M. BOCCALON Henri
Professeur Honoraire	M. BONAFÉ Jean-Louis
Professeur Honoraire	M. BONEU Bernard
Professeur Honoraire	M. BONNEVIALLE Paul
Professeur Honoraire	M. BOUNHOURE Jean-Paul
Professeur Honoraire	M. BOUTAULT Franck
Professeur Honoraire Associé	M. BROS Bernard
Professeur Honoraire	M. BUGAT Roland
Professeur Honoraire	M. CAHUZAC Jean-Philippe
Professeur Honoraire	M. CARATERO Claude
Professeur Honoraire	M. CARLES Pierre
Professeur Honoraire	M. CARON Philippe
Professeur Honoraire	M. CARRIERE Jean-Paul
Professeur Honoraire	M. CARTON Michel
Professeur Honoraire	M. CATHALA Bernard
Professeur Honoraire	M. CHABANON Gérard
Professeur Honoraire	M. CHAMONTIN Bernard
Professeur Honoraire	M. CHAP Hugues
Professeur Honoraire	M. CHAVOIN Jean-Pierre
Professeur Honoraire	M. CLANET Michel
Professeur Honoraire	M. CONTE Jean
Professeur Honoraire	M. COSTAGLIOLA Michel
Professeur Honoraire	M. COTONAT Jean
Professeur Honoraire	M. DABERNAT Henri
Professeur Honoraire	M. DAHAN Marcel
Professeur Honoraire	M. DALOUS Antoine
Professeur Honoraire	M. DALY-SCHVEITZER Nicolas
Professeur Honoraire	M. DAVID Jean-Frédéric
Professeur Honoraire	M. DELSOL Georges
Professeur Honoraire	Mme DELISLE Marie-Bernadette
Professeur Honoraire	Mme DIDIER Jacqueline
Professeur Honoraire	M. DUCOS Jean
Professeur Honoraire	M. DUFFAUT Michel
Professeur Honoraire	M. DUPRE M.
Professeur Honoraire	M. DURAND Dominique
Professeur Honoraire associé	M. DUTAU Guy
Professeur Honoraire	M. ESCHAPASSE Henri
Professeur Honoraire	M. ESCOURROU Jean
Professeur Honoraire	M. ESQUERRE J.P.
Professeur Honoraire	M. FABIÉ Michel
Professeur Honoraire	M. FABRE Jean
Professeur Honoraire	M. FOURNIAL Gérard
Professeur Honoraire	M. FOURNIE Bernard
Professeur Honoraire	M. FOURTANIER Gilles
Professeur Honoraire	M. FRAYSSE Bernard
Professeur Honoraire	M. FREXINOS Jacques
Professeur Honoraire	Mme GENESTAL Michèle
Professeur Honoraire	M. GERAUD Gilles
Professeur Honoraire	M. GHISOLFI Jacques
Professeur Honoraire	M. GLOCK Yves
Professeur Honoraire	M. GOUZI Jean-Louis
Professeur Honoraire	M. GRAND Alain
Professeur Honoraire	M. GUIRAUD CHAUMEIL Bernard
Professeur Honoraire	M. HOFF Jean
Professeur Honoraire	M. JOFFRE Francis
Professeur Honoraire	M. LAGARRIGUE Jacques
Professeur Honoraire	M. LANG Thierry
Professeur Honoraire	Mme LARENG Marie-Blanche
Professeur Honoraire	M. LAURENT Guy
Professeur Honoraire	M. LAZORTHES Franck
Professeur Honoraire	M. LAZORTHES Yves
Professeur Honoraire	M. LEOPHONTE Paul
Professeur Honoraire	M. MAGNAVAL Jean-François
Professeur Honoraire	M. MALECAZE François
Professeur Honoraire	M. MANELFE Claude
Professeur Honoraire	M. MANSAT Michel
Professeur Honoraire	M. MARCHOU Bruno
Professeur Honoraire	M. MASSIP Patrice
Professeur Honoraire	Mme MARTY Nicole
Professeur Honoraire	M. MAZIERES Bernard
Professeur Honoraire	M. MONROZIES Xavier
Professeur Honoraire	M. MOSCOVICI Jacques
Professeur Honoraire	M. MURAT
Professeur Honoraire associé	M. NICODEME Robert
Professeur Honoraire	M. OLIVES Jean-Pierre
Professeur Honoraire	M. PARINAUD Jean
Professeur Honoraire	M. PASCAL Jean-Pierre
Professeur Honoraire	M. PERRET Bertrand
Professeur Honoraire	M. PESSEY Jean-Jacques
Professeur Honoraire	M. PLANTE Pierre
Professeur Honoraire	M. PONTONNIER Georges
Professeur Honoraire	M. POURRAT Jacques
Professeur Honoraire	M. PRADERE Bernard
Professeur Honoraire	M. PRIS Jacques
Professeur Honoraire	Mme PUEL Jacqueline
Professeur Honoraire	M. PUEL Pierre
Professeur Honoraire	M. PUJOL Michel
Professeur Honoraire	M. QUERLEU Denis
Professeur Honoraire	M. RAILHAC Jean-Jacques
Professeur Honoraire	M. REGIS Henri
Professeur Honoraire	M. REGNIER Claude
Professeur Honoraire	M. REME Jean-Michel
Professeur Honoraire	M. RISCHMANN Pascal
Professeur Honoraire	M. RIVIERE Daniel
Professeur Honoraire	M. ROCHE Henri
Professeur Honoraire	M. ROCHICCIOLI Pierre
Professeur Honoraire	M. ROLLAND Michel
Professeur Honoraire	M. ROQUES-LATRILLE Christian
Professeur Honoraire	M. RUMEAU Jean-Louis
Professeur Honoraire	M. SALVADOR Michel
Professeur Honoraire	M. SALVAYRE Robert
Professeur Honoraire	M. SARRAMON Jean-Pierre
Professeur Honoraire	M. SERRE Guy
Professeur Honoraire	M. SIMON Jacques
Professeur Honoraire	M. SUC Jean-Michel
Professeur Honoraire	M. THOUVENOT Jean-Paul
Professeur Honoraire	M. TREMOULET Michel
Professeur Honoraire	M. VALDIGUIE Pierre
Professeur Honoraire	M. VAYSSE Philippe
Professeur Honoraire	M. VINEL Jean-Pierre
Professeur Honoraire	M. VIRENQUE Christian
Professeur Honoraire	M. VOIGT Jean-Jacques

Professeurs Emérites

Professeur ARLET Philippe
Professeur BOUTAULT Franck
Professeur CARON Philippe
Professeur CHAMONTIN Bernard
Professeur CHAP Hugues
Professeur GRAND Alain
Professeur LAGARRIGUE Jacques
Professeur LAURENT Guy
Professeur LAZORTHES Yves
Professeur MAGNAVAL Jean-François
Professeur MARCHOU Bruno
Professeur PERRET Bertrand
Professeur RISCHMANN Pascal
Professeur RIVIERE Daniel
Professeur ROUGE Daniel

FACULTE DE SANTE
Département Médecine Maieutique et Paramédicaux

P.U. - P.H.
Classe Exceptionnelle et 1ère classe

M. ACAR Philippe	Pédiatrie
M. ACCADBLED Franck (C.E)	Chirurgie Infantile
M. ALRIC Laurent (C.E)	Médecine Interne
M. AMAR Jacques	Thérapeutique
Mme ANDRIEU Sandrine	Epidémiologie, Santé publique
M. ARBUS Christophe	Psychiatrie
M. ARNAL Jean-François (C.E)	Physiologie
M. ATTAL Michel (C.E)	Hématologie
M. AVET-LOISEAU Hervé	Hématologie, transfusion
M. BERRY Antoine	Parasitologie
Mme BERRY Isabelle (C.E)	Biophysique
M. BIRMES Philippe	Psychiatrie
M. BONNEVILLE Fabrice	Radiologie
M. BOSSAVY Jean-Pierre (C.E)	Chirurgie Vasculaire
M. BRASSAT David	Neurologie
M. BROUCHET Laurent	Chirurgie thoracique et cardio-vascul
M. BROUSSET Pierre (C.E)	Anatomie pathologique
M. BUJAN Louis (C. E)	Urologie-Andrologie
Mme BURA-RIVIERE Alessandra (C.E)	Médecine Vasculaire
M. BUREAU Christophe	Hépato-Gastro-Entérologie
M. BUSCAIL Louis (C.E)	Hépato-Gastro-Entérologie
M. CALVAS Patrick (C.E)	Génétique
M. CANTAGREL Alain (C.E)	Rhumatologie
M. CARRERE Nicolas	Chirurgie Générale
M. CARRIE Didier (C.E)	Cardiologie
M. CHAIX Yves	Pédiatrie
Mme CHARPENTIER Sandrine	Médecine d'urgence
M. CHAUFOUR Xavier	Chirurgie Vasculaire
M. CHAUVEAU Dominique	Néphrologie
M. CHAYNES Patrick	Anatomie
M. CHIRON Philippe (C.E)	Chir. Orthopédique et Traumatologie
M. CHOLLET François (C.E)	Neurologie
M. CONSTANTIN Arnaud	Rhumatologie
M. COURBON Frédéric	Biophysique
Mme COURTADE SAIDI Monique (C.E)	Histologie Embryologie
M. DAMBRIN Camille	Chir. Thoracique et Cardiovasculaire
M. DE BOISSEZON Xavier	Médecine Physique et Réadapt Fonct.
M. DEGUINE Olivier (C.E)	Oto-rhino-laryngologie
M. DELABESSE Eric	Hématologie
M. DELOBEL Pierre	Maladies Infectieuses
M. DELORD Jean-Pierre (C.E)	Cancérologie
M. DIDIER Alain (C.E)	Pneumologie
M. DUCOMMUN Bernard	Cancérologie
Mme DULY-BOUHANICK Béatrice (C.E)	Thérapeutique
M. ELBAZ Meyer	Cardiologie
M. FERRIERES Jean (C.E)	Epidémiologie, Santé Publique
M. FOURCADE Olivier	Anesthésiologie
M. FOURNIÉ Pierre	Ophtalmologie
M. GALINIER Michel (C.E)	Cardiologie
M. GAME Xavier	Urologie
Mme GARDETTE Virginie	Epidémiologie, Santé publique
M. GEERAERTS Thomas	Anesthésiologie et réanimation
Mme GOMEZ-BROUCHET Anne-Muriel	Anatomie Pathologique
M. GOURDY Pierre (C.E)	Endocrinologie
M. GROLLEAU RAOUX Jean-Louis (C.E)	Chirurgie plastique
Mme GUIMBAUD Rosine	Cancérologie
Mme HANAIRE Hélène (C.E)	Endocrinologie
M. HUYGHE Eric	Urologie
M. IZOPET Jacques (C.E)	Bactériologie-Virologie
M. KAMAR Nassim (C.E)	Néphrologie

P.U. Médecine générale
M. OUSTRIC Stéphane (C.E)

Mme LAMANT Laurence (C.E)	Anatomie Pathologique
M. LANGIN Dominique (C.E)	Nutrition
Mme LAPRIE Anne	Radiothérapie
M. LARRUE Vincent	Neurologie
M. LAUQUE Dominique (C.E)	Médecine d'Urgence
M. LAUWERS Frédéric	Chirurgie maxillo-faciale
M. LEOBON Bertrand	Chirurgie Thoracique et Cardio-vasculaire
M. LEVADE Thierry (C.E)	Biochimie
M. LIBLAU Roland (C.E)	Immunologie
M. MALAVAUD Bernard	Urologie
M. MANSAT Pierre	Chirurgie Orthopédique
M. MARQUE Philippe (C.E)	Médecine Physique et Réadaptation
M. MAS Emmanuel	Pédiatrie
M. MAURY Jean-Philippe (C.E)	Cardiologie
Mme MAZEREEUW Juliette	Dermatologie
M. MAZIERES Julien (C.E)	Pneumologie
M. MINVILLE Vincent	Anesthésiologie Réanimation
M. MOLINIER Laurent (C.E)	Epidémiologie, Santé Publique
M. MONTASTRUC Jean-Louis (C.E)	Pharmacologie
Mme MOYAL Elisabeth (C.E)	Cancérologie
M. MUSCARI Fabrice	Chirurgie Digestive
Mme NOURHASHEMI Fatemeh (C.E)	Gériatrie
M. OLIVOT Jean-Marc	Neurologie
M. OSWALD Eric (C.E)	Bactériologie-Virologie
M. PARIENTE Jérémie	Neurologie
M. PAUL Carle (C.E)	Dermatologie
M. PAYOUX Pierre (C.E)	Biophysique
M. PAYRASTRE Bernard (C.E)	Hématologie
M. PERON Jean-Marie (C.E)	Hépato-Gastro-Entérologie
M. RASCOL Olivier (C.E)	Pharmacologie
Mme RAUZY Odile	Médecine Interne
M. RAYNAUD Jean-Philippe (C.E)	Psychiatrie Infantile
M. RECHER Christian(C.E)	Hématologie
M. RITZ Patrick (C.E)	Nutrition
M. ROLLAND Yves (C.E)	Gériatrie
M. RONCALLI Jérôme	Cardiologie
M. ROUGE Daniel (C.E)	Médecine Légale
M. ROUSSEAU Hervé (C.E)	Radiologie
M. ROUX Franck-Emmanuel	Neurochirurgie
M. SAILLER Laurent (C.E)	Médecine Interne
M. SALES DE GAUZY Jérôme (C.E)	Chirurgie Infantile
M. SALLES Jean-Pierre (C.E)	Pédiatrie
M. SANS Nicolas	Radiologie
M. SCHMITT Laurent (C.E)	Psychiatrie
Mme SELVES Janick (C.E)	Anatomie et cytologie pathologiques
M. SENARD Jean-Michel (C.E)	Pharmacologie
M. SERRANO Elie (C.E)	Oto-rhino-laryngologie
M. SIZUN Jacques (C.E)	Pédiatrie
M. SOL Jean-Christophe	Neurochirurgie
Mme SOTO-MARTIN Maria-Eugénia	Gériatrie et biologie du vieillissement
M. SOULAT Jean-Marc	Médecine du Travail
M. SOULIE Michel (C.E)	Urologie
M. SUC Bertrand	Chirurgie Digestive
Mme TAUBER Marie-Thérèse (C.E)	Pédiatrie
M. TELMON Norbert (C.E)	Médecine Légale
Mme TREMOLLIERES Florence	Biologie du développement
Mme URO-COSTE Emmanuelle (C.E)	Anatomie Pathologique
M. VAYSSIERE Christophe (C.E)	Gynécologie Obstétrique
M. VELLAS Bruno (C.E)	Gériatrie
M. VERGEZ Sébastien	Oto-rhino-laryngologie

FACULTE DE SANTE
Département Médecine Maieutique et Paramédicaux

P.U. - P.H.
2ème classe

M. ABBO Olivier	Chirurgie infantile
M. AUSSEIL Jérôme	Biochimie et biologie moléculaire
Mme BONGARD Vanina	Epidémiologie, Santé publique
M. BONNEVIALLE Nicolas	Chirurgie orthopédique et traumatologique
M. BOUNES Vincent	Médecine d'urgence
Mme BOURNET Barbara	Gastro-entérologie
Mme CASPER Charlotte	Pédiatrie
M. CAVAIGNAC Etienne	Chirurgie orthopédique et traumatologie
M. CHAPUT Benoit	Chirurgie plastique
M. COGNARD Christophe	Radiologie
Mme CORRE Jill	Hématologie
Mme DALENC Florence	Cancérologie
M. DE BONNECAZE Guillaume	Anatomie
M. DECRAMER Stéphane	Pédiatrie
M. EDOUARD Thomas	Pédiatrie
M. FAGUER Stanislas	Néphrologie
Mme FARUCH BILFELD Marie	Radiologie et imagerie médicale
M. FRANCHITTO Nicolas	Addictologie
M. GARRIDO-STÖWHAS Ignacio	Chirurgie Plastique
M. GUIBERT Nicolas	Pneumologie
M. GUILLEMINAULT Laurent	Pneumologie
M. HERIN Fabrice	Médecine et santé au travail
M. LAIREZ Olivier	Biophysique et médecine nucléaire
M. LAROCHE Michel	Rhumatologie
Mme LAURENT Camille	Anatomie Pathologique
M. LE CAIGNEC Cédric	Génétique
M. LEANDRI Roger	Biologie du dével. et de la reproduction
M. LOPEZ Raphael	Anatomie
M. MARCHEIX Bertrand	Chirurgie thoracique et cardiovasculaire
M. MARTIN-BLONDEL Guillaume	Maladies infectieuses, maladies tropicales
Mme MARTINEZ Alejandra	Gynécologie
M. MARX Mathieu	Oto-rhino-laryngologie
M. MEYER Nicolas	Dermatologie
M. PAGES Jean-Christophe	Biologie cellulaire
Mme PASQUET Marlène	Pédiatrie
M. PORTIER Guillaume	Chirurgie Digestive
M. PUGNET Grégory	Médecine interne
M. REINA Nicolas	Chirurgie orthopédique et traumatologique
M. RENAUDINEAU Yves	Immunologie
Mme RUYSSEN-WITRAND Adeline	Rhumatologie
Mme SAVAGNER Frédérique	Biochimie et biologie moléculaire
M. SAVALL Frédéric	Médecine légale
M. SILVA SIFONTES Stein	Réanimation
M. SOLER Vincent	Ophtalmologie
Mme SOMMET Agnès	Pharmacologie
M. TACK Ivan	Physiologie
Mme VAYSSE Charlotte	Cancérologie
Mme VEZZOSI Delphine	Endocrinologie
M. YRONDI Antoine	Psychiatrie
M. YSEBAERT Loic	Hématologie

P.U. Médecine générale
M. MESTHÉ Pierre
Mme ROUGE-BUGAT Marie-Eve

Professeurs Associés

Professeur Associé de Médecine Générale
M. ABITTEBOUL Yves
Mme BOURGEOIS Odile
M. BOYER Pierre
M. CHICOULAA Bruno
Mme IRI-DELAHAYE Motoko
M. PIPONNIER David
M. POUTRAIN Jean-Christophe
M. STILLMUNKES André

Professeur Associé de Bactériologie-Hygiène
Mme MALAVAUD Sandra

FACULTE DE SANTE
Département Médecine Maieutique et Paramédicaux

MCU - PH

Mme ABRAVANEL Florence	Bactériologie Virologie Hygiène
M. APOIL Pol Andre	Immunologie
Mme ARNAUD Catherine	Epidémiologie
Mme AUSSEIL-TRUDEL Stéphanie	Biochimie
Mme BASSET Céline	Cytologie et histologie
Mme BELLIERES-FABRE Julie	Néphrologie
Mme BERTOLI Sarah	Hématologie, transfusion
M. BIETH Eric	Génétique
Mme BREHIN Camille	Pneumologie
M. BUSCAIL Etienne	Chirurgie viscérale et digestive
Mme CAMARE Caroline	Biochimie et biologie moléculaire
M. CAMBUS Jean-Pierre	Hématologie
Mme CANTERO Anne-Valérie	Biochimie
Mme CARFAGNA Luana	Pédiatrie
Mme CASPAR BAUGUIL Sylvie	Nutrition
Mme CASSAGNE Myriam	Ophtalmologie
Mme CASSAING Sophie	Parasitologie
Mme CASSOL Emmanuelle	Biophysique
Mme CHANTALAT Elodie	Anatomie
M. CHASSAING Nicolas	Génétique
M. CLAVEL Cyril	Biologie Cellulaire
Mme COLOMBAT Magali	Anatomie et cytologie pathologiques
M. CONGY Nicolas	Immunologie
Mme COURBON Christine	Pharmacologie
M. CUROT Jonathan	Neurologie
Mme DAMASE Christine	Pharmacologie
Mme DE GLISEZENSKY Isabelle	Physiologie
M. DEDOUIT Fabrice	Médecine Légale
M. DEGBOE Yannick	Rhumatologie
M. DELMAS Clément	Cardiologie
M. DELPLA Pierre-André	Médecine Légale
M. DESPAS Fabien	Pharmacologie
M. DUBOIS Damien	Bactériologie Virologie Hygiène
Mme ESQUIROL Yolande	Médecine du travail
Mme EVRARD Solène	Histologie, embryologie et cytologie
Mme FILLAUX Judith	Parasitologie
Mme FLOCH Pauline	Bactériologie-Virologie
Mme GALINIER Anne	Nutrition
Mme GALLINI Adeline	Epidémiologie
M. GANTET Pierre	Biophysique
M. GASQ David	Physiologie
M. GATIMEL Nicolas	Médecine de la reproduction

M.C.U. Médecine générale

M. BISMUTH Michel
M. BRILLAC Thierry
Mme DUPOUY Julie
M. ESCOURROU Emile

Mme GENNERO Isabelle	Biochimie
Mme GENOUX Annelise	Biochimie et biologie moléculaire
Mme GRARE Marion	Bactériologie Virologie Hygiène
M. GUERBY Paul	Gynécologie-Obstétrique
Mme GUILBEAU-FRUGIER Céline	Anatomie Pathologique
Mme GUYONNET Sophie	Nutrition
M. HAMDI Safouane	Biochimie
Mme HITZEL Anne	Biophysique
Mme INGUENEAU Cécile	Biochimie
M. IRIART Xavier	Parasitologie et mycologie
Mme JONCA Nathalie	Biologie cellulaire
M. KIRZIN Sylvain	Chirurgie générale
Mme LAPEYRE-MESTRE Maryse	Pharmacologie
M. LEPAGE Benoit	Biostatistiques et Informatique médicale
M. LHERMUSIER Thibault	Cardiologie
M. LHOMME Sébastien	Bactériologie-virologie
Mme MASSIP Clémence	Bactériologie-virologie
Mme MAUPAS SCHWALM Françoise	Biochimie
Mme MONTASTIER Emilie	Nutrition
M. MONTASTRUC François	Pharmacologie
Mme MOREAU Jessika	Biologie du dév. Et de la reproduction
Mme MOREAU Marion	Physiologie
M. MOULIS Guillaume	Médecine interne
Mme NASR Nathalie	Neurologie
Mme NOGUEIRA M.L.	Biologie Cellulaire
Mme PERROT Aurore	Hématologie
M. PILLARD Fabien	Physiologie
Mme PLAISANCIE Julie	Génétique
Mme PUISSANT Bénédicte	Immunologie
Mme QUELVEN Isabelle	Biophysique et médecine nucléaire
Mme RAYMOND Stéphanie	Bactériologie Virologie Hygiène
M. REVET Alexis	Pédo-psychiatrie
M. RIMAILHO Jacques	Anatomie et Chirurgie Générale
Mme SABOURDY Frédérique	Biochimie
Mme SAUNE Karine	Bactériologie Virologie
Mme SIEGFRIED Aurore	Anatomie et cytologie pathologiques
M. TAFANI Jean-André	Biophysique
M. TREINER Emmanuel	Immunologie
Mme VALLET Marion	Physiologie
M. VERGEZ François	Hématologie
Mme VIJA Lavinia	Biophysique et médecine nucléaire

Maîtres de Conférence Associés

M.C.A. Médecine Générale

M. BIREBENT Jordan
Mme BOUSSIER Nathalie
Mme FREYENS Anne
Mme LATROUS Leila
Mme PUECH Marielle

REMERCIEMENTS AU JURY

Professeur Silva, vous me faites l'honneur de présider ce jury. Je vous remercie de m'avoir accueilli au sein de cette nouvelle spécialité et pour cette si belle maquette d'internat ; vous êtes pour moi une référence en termes de connaissances et par l'intérêt scientifique que vous portez à cette discipline.

Amazigh, merci d'avoir accepté de m'encadrer en dernier lieu dans cette thèse, avec pragmatisme. J'ai eu la chance de t'avoir comme interne séniorisé en premier semestre et directeur de thèse en dernier.

Dr Riu, merci de m'avoir accueilli dans votre service, avec un regard rassurant, en premier semestre quand j'étais encore toute jeune et timide.

Clément, à la vivacité intellectuelle surprenante, un grand merci pour cette maquette orientée vers la cardiologie. J'espère que je serai à la hauteur au semestre prochain.

Fanny, tu es un autre bel exemple de vivacité et d'efficacité ; le tout sur un fond d'humanité. Je te souhaite une belle carrière universitaire.

Caroline, c'est bien la première fois que je t'appelle ainsi ! Tu m'as suivi au cours de mon internat avec bienveillance, tu es une référence pour moi en termes de cardiologie, de réanimation et d'efficacité sans fioriture. A bientôt à l'USIC !

REMERCIEMENTS PERSONNELS

A ma famille,

A mes parents, qui m'ont encadré bien plus que le temps de la thèse… Je vous aime.

A mes sœurs, la grande Chloé et la petite Alice (les 3 biquettes), qui sont maintenant 2 chouettes femmes. Merci Chloé et Cyril pour tous les moments partagés à Tarbes, en montagne (et cette chambre d'un rose éclatant). J'apprécie être le petit courant d'air qui passe de temps à autre chez vous. Et la brillante Alice, reine de l'anticipation, qui prend le relais de l'internat, courage !

A mon grand-père Léon et ce havre de paix de Lodonnec, qui ont embellis tous mes étés depuis l'enfance et bien plus … Je t'embrasse.

A mes grands-parents Colette et Bernard,

A mes cousins, cousines, Grégoire, Camille et Antoine

A mes oncles et tantes, Benoit, Paule, Magalie

A Thierry, Isa ; l'atmosphère de Nexon, du Sirque, du Raku, de la céramique, du jardin …

A la fanfare et la musique,

A La Vaginale qui a été une rencontre fabuleuse et qui a permis et justifié plein de belles choses

Au VGB qui ont pris le relais, et à la prochaine fanfare

A Aurèle, qui m'a donné le coup de pouce au bon moment

A la promo du bureau, Marie, Clara, Julie, Yacine, Agathe, Laureen, Rosine et le K barré du cirque plein d'air.

Et puis, Starfoufou, Guizmo, Nadir, Adama, Charles, Pipo, Dylou, Yoda, Jim, Louis, Jonas, encore Aurèle, Alex, Léa, Camille, Antoin, Hortense, Lise, Louise, Côme, Sirob, Rodger, Loulou, Kiki, Abde, Juliette, Jean Loup, Saïmon, PA ; et à tous ces joyeux fanfarons.

Aux amis,

A Agathe, j'ai de la chance de t'avoir parmi mes plus proches complices et d'avoir partagé plein de beaux moments et voyages avec toi. Tu es une jolie femme pleine de finesse et de poésie. A toutes les prochaines occasions, et à Nadir qui te va si bien !

A Blandine, la grande binôme du lycée et de 2 années de colocation, ta pétillante personnalité illumine tous nos moments.

A Julie, j'ai une immense tendresse pour toi ; ton sourire, tes goûts et ta personnalité délicates. A tous nos questionnements sans réponse, nos incertitudes, nos choix impossibles… Et merci pour le soutien des 6 derniers mois.

A Marie, qui est un brin de femme impressionnant ; qui te montre que beaucoup de choses sont réalisables si tu y crois et que tu te donnes… A nos retrouvailles étincelantes à Paris et aux prochaines !

A Clem, le moussaillon par excellence de nos voyages, généreuse et vivante.

A Clara, petite plante vivace, et à toutes nos soirées bien arrosées, tu es une belle amie.

A Camille et à Antoine, qui sont devenus les deux meilleurs amis toulousains de la fanfare ; vous retrouvez à Toulouse a toujours une saveur particulière.

A Asmaâ et à Oman,

Aux amis d'enfance, Béren, Ana, Julia, Justine.

Aux amis du lycée, Audrey, Blandine, Juanito, Thomas, Andy, Benoit, Aurélie, Ethan, Romane, Marion ; nous avons parcourus un magnifique bout de chemin de adolescent à « à peine adulte » ensemble, semé d'embuches et de soirées expérimentales.

Aux copains de la fac, Gaby, Norman, Clément, Clara, Agathe, Alizée, Guillaume, Margaux, Lou ; on aura bien usés les pavés de la place Plumereau (… et les sièges de Cloch) !

Aux amis de mes parents qui sont devenus aussi mes amis, toujours d'une grande générosité, Marie-Paule, Jean Paul, Andréa, Ricardo, Dodue, Cricri, Thierry, Brigitte, Henri, Jean Mi, Marie …

A mes colocs ; le binôme Marine (et son « bon » typique qui ponctue nos discussions entre autre sur le balcon) et Axelle ; à Lise (et le chat imaginaire)

Au semestre à l'USIC qui aura été un semestre central dans mon internat ; à Clémence qui m'aura beaucoup appris (entre autre l'écho pragmatique) ; à Caro et Clément ; aux internes et amis Laure, Thibault, Laurence, Alex, Henri, vous avez été tous les cinq importants pour moi.

Au semestre à Cahors, la team de Tenerife : Marion, Pauline, Lise ainsi que Joris (et sa bêtise), Albert, Basile,

Au semestre au SMIT, à l'équipe de foot Marine, Asmaâ, Francis, Nico, Erwan, Natasha ; et à leurs chefs Gaspard, Lydie, Mumu, Camille, Alexa, GMB, Lucie.

A Lydie, pour sa bienveillance et son soutien

Au semestre en Réa Poly Rangueil, à Elena (petit rayon de soleil, à tous les moments du BRR dont on rit encore) , Raph, Albin, Justine … et leurs chefs, entre autre, Laure, Max, Antoine (pour cette pose de JJ sous ECMO en chambre), Fanny, Christelle.

A la petite famille de la Pitié, Asma, Le Transporteur, Sofia, Zozo, Louise, Tim, Juliette, Alex, Ouriel, Lucie, Petra, David, Juliette, Mathieu Schmidt.

Au semestre qui n'est pas encore terminé, au fabuleux trinôme des petits potes, Julie et Toto + le bip ; à Anna qui m'a épaulé depuis le début ; aux chefs de la Réanimation UTO2, Laurence, MarieB, Chloé, Olivier, Stan qui forment une belle équipe ; aux autres chefs du DNTO, Eloise,

Pierre, Clotilde, David… ; aux jeunes internes, Camille et Delphine qui ont déjà un très bel état d'esprit.

A tous les IDE et paramédicaux que j'ai pu croiser à un moment au cours de mon internat et qui sont investis dans leur travail.

Et enfin, à mes bâtons de ski et de randonnée qui m'ont beaucoup soutenu d'une manière différente …

TABLE OF CONTENTS

ABBREVIATIONS

ARF : acute respiratory failure

AUC : area under the curve

BA : Bresenham's algorithm

CE : cross entropy

CNN : convolutional neural network

CRX : chest X ray

CT : computerized tomography

DL : deep learning

Grad CAM : Gradient weighted Class Activation Mapping

ICU : intensive care unit

LPT : pleural line thickening

LUS : lung ultrasound

ML : machine learning

PE : pleural effusion

ROC : receiving operating characteristic curve

RT PCR : real-time reverse transcription polymerase-chain-reaction

ABSTRACT

Context : COVID 19 pandemic has highlighted the need to combine non-invasive, rapid, and widely available imaging techniques to achieve a successful early detection and surveillance of the disease. Machine learning algorithms appears to be promising for the analysis of LUS images.

Purpose : To develop a performant algorithm using artificial intelligence capable of identifying LUS abnormalities in a patient with Covid-19 pneumonia

Methods : This is an prospective study in Toulouse University Hospital and Cayenne hospital. 58 patients were included between June 2020 and March 2021. Inclusion criteria were COVID 19 confirmed with RT PCR and acute respiratory failure at hospital admission. Every patient included underwent LUS assessment by one of the three investigators (expert in LUS). Images were gathered and LUS frames were labeled by those same investigators. Semantic segmentation method was used with 4 convolutional neural networks tested.

To evaluate the different architecture, metrics and ROC curve were computed. A confusion matrix was also design.

For B superclass, we used post processing tool based on signal analysis and Bresenham's algorithm to discriminate the type of B lines. This method was evaluated with Grad CAM.

For external validation, the semantic segmentation network was tested on POCUS dataset.

Results : In total, 5 000 LUS frames were labeled from 58 patients affected by COVID 19 with different degree of severity. Those 5 000 frames were divided in 5 fold : 4 for training and 1 for validation. DeepLab appears to be the better segmentation model in Recall and F1. ROC curve using DeepLab model showed AUC at 0.96 for A pattern ; 0,97 for B superclass ; 0,95 for C pattern.

Conclusion : DeepLab segmentation was successful to identify clinically meaningful LUS patterns from COVID 19 patient's dataset.

KEYWORDS : Lung ultrasound ; Covid 19 ; deep learning ; semantic segmentation ; convolution neural network

GLOSSARY

Artificial Intelligence : simulation of human intelligence processes by machines, especially computer systems.

Machine Learning : method of data analysis that automates analytical model building ; based on the idea that systems can learn from data, identify patterns and make decisions with minimal human intervention.

Deep Learning : type of machine learning concerned with algorithms inspired by the functioning of human neurons. The system is designed into a multitude of interconnected layers each receiving and interpreting information from previous layer.

Semantic segmentation : process to label each pixel of an image with corresponding class of what is being represented. It makes possible to recognize a set of pixels that form distinct categories.

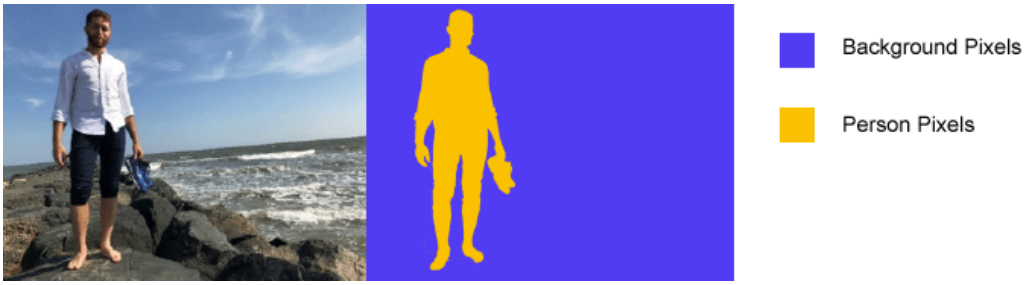

Source : https://fr.mathworks.com/

Convolutional Neural Network (CNN)

Network architecture which learns directly from data, eliminating the need for manual feature extraction. Useful for finding patterns in images to recognize objects.

CNN is composed of an input layer, output layer and many hidden layers in between.

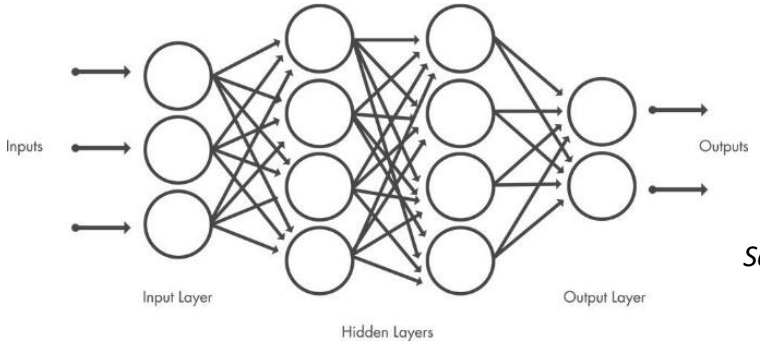

Source : https://mathworks.com

Two main steps are required :

1) **Convolution** :

- Purpose : to extract characteristics specific to each image by compressing them in order to reduce their initial size.
- Principle : the image provided as input passes through a succession of filters, creating at the same time new images called convolution maps or activation map. The resulting convolution maps are linked in a feature vector called CNN code. The objective is to reduce the number of parameters that the network needs to learn.

After learning features in many layers, the architecture of a CNN shifts to classification.

2) **Classification :**

- Purpose : to combine the characteristics of the CNN code in order to classify the image.
- Principle : the CNN code obtained at the output of the convolutional part is provided as input in a second part, consisting of fully connected layer (called multilayer perceptron). The output of the connected layer is a vector of K dimensions where K is the number of classes. The vector contains the probabilities for each class of any image being classified.

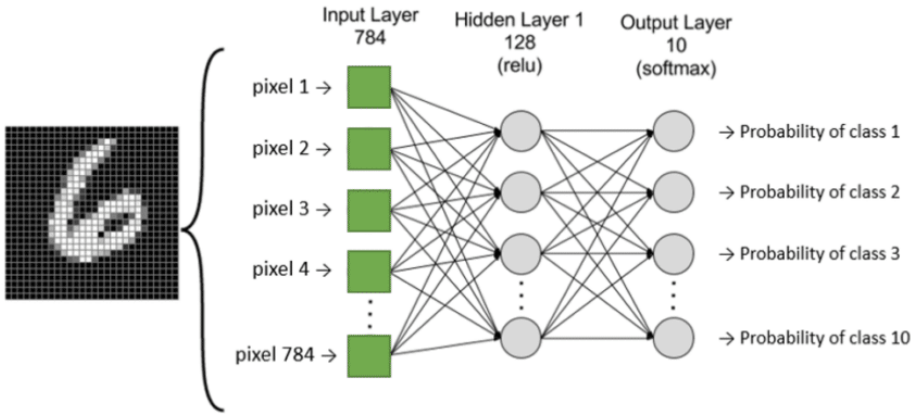

Source : https://datascientest.com/

Cross Entropy Loss : mathematical method to minimize the difference between the predicted distribution and the true distribution ; quantifies the error and minimizes it.

Metrics : evaluation of a Deep Learning algorithm :

- **F1 Metric :** is the harmonic mean of precision (specificity) and recall (sensitivity) ; F1 score is high if Precision and Recall are high

$$F1\ score = 2 * \frac{Precision\ * Recall}{Precision + Recall}$$

- **Precision :** highlights well classified pixels that are not outside of patterns region ; equivalent to specificity
- **Recall :** shows if all pixel belonging to patterns are found ; equivalent to sensibility (high recall succeeds well in finding all positive cases)
- **Confusion matrix :** the matrix compares the actual target values with those predicted by the machine learning. This gives a view of how well our classification model is performing and what kinds of errors it is making.

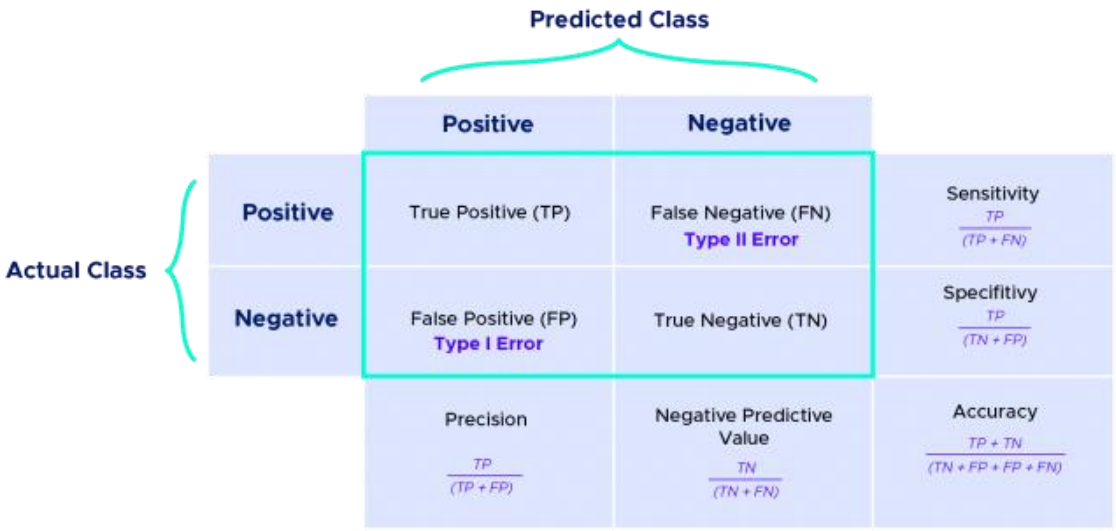

Source : https://datascientest.com/

Gradient weighted Class Activation Mapping (Grad CAM) : technique for visualizing the regions of input that are « important » for decisions / predictions from a large class of CNN-based models, making them more transparent. This approach uses the gradients of any target output, flowing into the final convolutional layer to produce a localization map highlighting the important regions in the image for predicting the outcome.

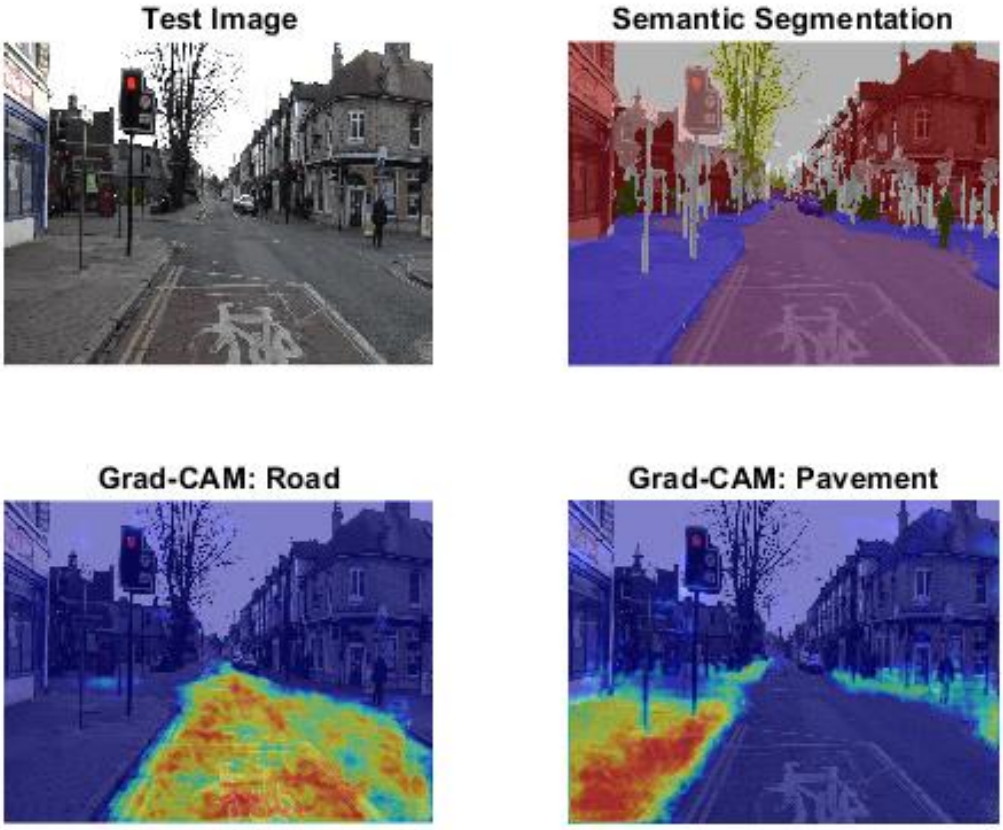

Source : https://datascientest.com/

INTRODUCTION

The world-wide outbreak of the novel coronavirus disease (COVID-19) has highlighted the need to combine non-invasive, rapid, and widely available imaging techniques to achieve a successful early detection and surveillance of the disease. Imaging has a key role to play in the diagnostic pathway and lung ultrasound (LUS) might play an important role.

LUS SEMIOTICS

LUS findings remain on the interpretation of artefacts produced at the pleural surface. It is true that LUS cannot been used for the evaluation of the pulmonary parenchyma in healthy patient due to the presence of air near the surrounding tissues, providing a high acoustic mismatch and a full reflection of the ultrasound beam. In this case, the pleural line (PL) appears as a thin echogenic line due to the elevated impedance at the interface between the superficial soft-tissues and the air in the lung. Nevertheless, some lung pathologies can reduce the impedance mismatch at the pleural surface and ultrasound beam can experiment relative reflection, refraction and attenuation, leading to so-called artifacts in LUS imagery.

LUS requires the knowledge of the following artifacts (1) :

- **A-line :** in sane patients, this artifact is produced by the beam reflection between the pleural line and the ultrasound probe. A-lines appeared as hyperechoic, horizontal lines arising at regular intervals from the pleural line, up to the bottom of the image
- **B-line :** B-lines are comet-tail artifacts, defined as discrete laser-like vertical hyperechoic reverberation artifacts arising from the pleural line and extending up to the bottom of the image without fading. B-lines are features of an abnormal lung condition. Thin B-Lines (B1), large B-Lines (B2), multiple B-lines and white lung pattern (B3) can be observed.
- **C-pattern:** Compared to normal lung, consolidation (C) on LUS replace the pleural line pattern with a relatively hypoechoic heterogeneous echo texture. Clinician can use these patterns (artifacts) to qualitatively diagnose the severity of a COVID-19 patient
- **Pleural effusion** : hypoechoic texture between pleural line and lung which appears atelectatic and hyperechoic

The interest of ultrasound for lung acute pathology was demonstrated by Lichtenstein *et al* in a study published in 2008 (2). Bedside LUS showed an accuracy of 90.5% in diagnosing the cause of acute respiratory failure in critically ill patients. The BLUE protocol has higher sensitivity, specificity and diagnostic accuracy for pleural effusions, alveolar consolidation and interstitial syndromes all the values for LUS are between 92% and 100%.

LUS AND COVID-19 INFECTION

COVID-19 causes clear and typical ultrasonographic patterns (3,4) , as shown in Figure 1. B lines in COVID-19 occurs in large numbers, both in separate and coalescent forms (light-beam patterns), and can give the appearance of a shining white lung. Irregularity of the pleural line, sub-pleural pulmonary consolidations and poor blood flow also occur in bilateral patchy clusters, and are mainly visible in the posterior and inferior areas.

In this regard, LUS has shown promise but its potential may be destined to evolve. Indeed, despite the fact that accumulating evidence suggest that LUS gives results that are similar to chest CT for evaluation of COVID-19 severity, it is broadly acknowledged that current LUS data interpretation, which is based only on medical experts' analysis, can be time-consuming, user-dependent, and hold the risk of leading to oversimplified diagnosis. To accurately cope with these issues, computer vision approaches, built upon machine learning algorithms have been recently proposed but have demonstrated variable classifier's accuracy and the poor explicability of the obtained results appears to be still a significant drawback. Moreover, the vast majority of the reported studies have only provided binary classifications (5), seeking either to disentangle the diagnosis of COVID-19 from alternative causes of acute respiratory failure or to assist on the identification of only one specific LUS patterns.

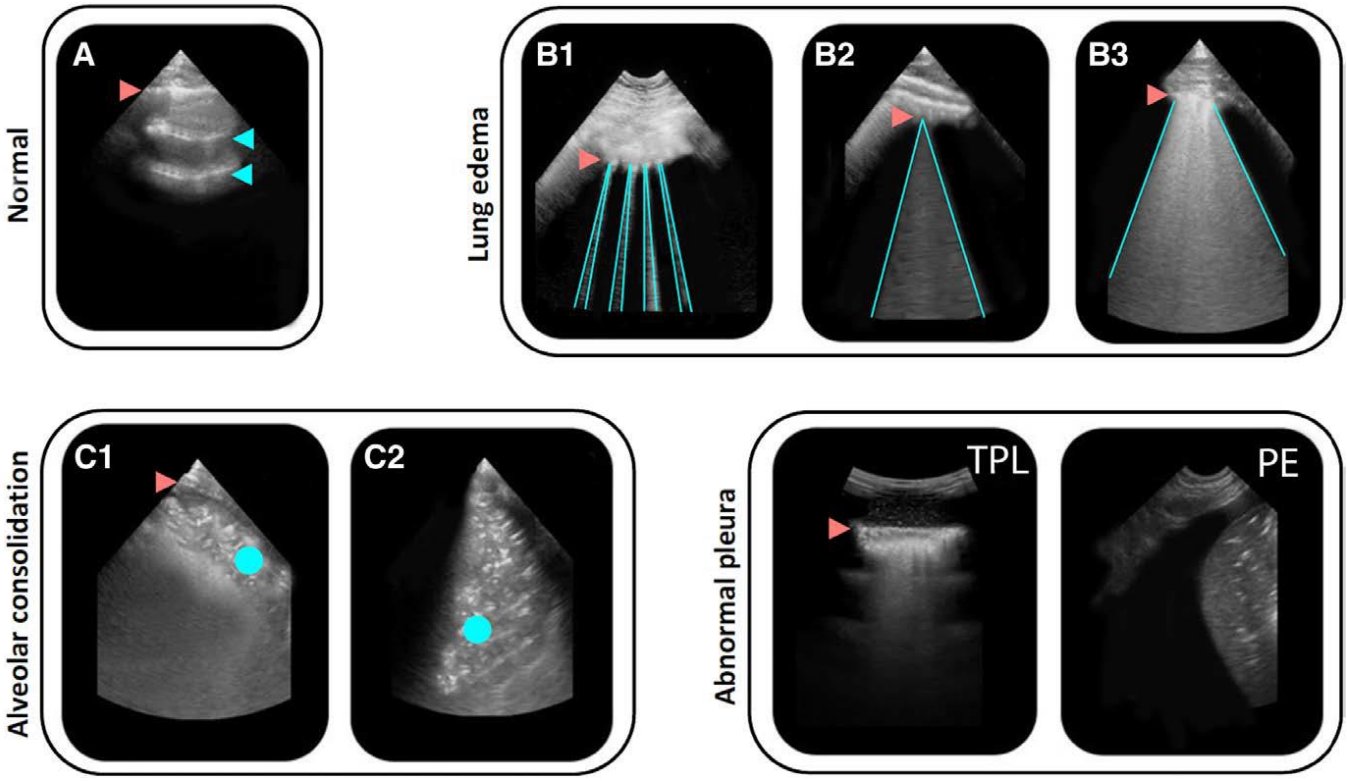

Fig. 1 : Lung ultrasound patterns (adapted from (6))

PLACE OF ULTRASOUND AMONG OTHER IMAGING

Computed Tomography (CT) was used as the main standard to identify lung pathology.

Use of chest CT comes with significant drawbacks : it is costly, exposes patients to radiation. In a triage protocol with massive patient flow, little CT equipment is available, patients may not be carried to dedicated CT room, equipment is hard to sterilize. Even if the LUS image quality is below CT quality, LUS may be an effective tool to predict severity and the need to admit patients with COVID-19 to the Intensive Care Unit (ICU) (6) .

Poggiali et al. found strong correlation between similar ultrasound findings and concurrent CT (7) . Twelve patients with COVID-19 underwent both LUS and CT scanning. All patients had diffuse B−lines with spared areas. Three had posterior subpleural consolidations and four had the appearance of organizing pneumonias: bilateral patchy subpleural or peripheral consolidations. CT scans confirmed bilateral lung involvement with ground-glass opacities and consolidation changes in all patients.

Regarding diagnostic performance of LUS compared to CXR or CT scan, a meta-analysis published in 2014 (8). showed pooled sensitivity and specificity for the diagnosis of pneumonia 94 and 96% respectively and area-under-the ROC curve of 0,99.

DEEP LEARNING – ARTIFICIAL INTELLIGENCE

With the rise of deep learning techniques, medical imagery has increasingly claimed attention for the computed assisted analysis. In particular the use of convolutional neural networks (CNNs) has led to substantial performance gain over the classic machine learning techniques. Multiples usages have been evaluated, especially for thoracic imaging (9). Several works on CT scans and Covid-19 infection have been recently published and have shown promising results in terms of :

- quantification and segmentation the infection with potential application such as severity prediction (10,11).
- performance in identifying COVID-19 from other pneumonia ; and stratifying patients into high- and low-risk groups (12).

Interpreting ultrasound images is user-dependent and it can lead to errors. To accurately cope with these issues, computer vision approaches seems to be relevant. In the specific setting of LUS data analysis from COVID-19 patients, an increasing number of ML architectures have been developed. They were able to achieve fairly high accuracy to differentiate the COVID-19 patients from both bacterial-related and other pneumonia cases and grade the pathology severity. But these methods have demonstrated variable classifier's accuracy (as shown in supplementary table 1, adapted from *Review of Machine Learning in Lung Ultrasound in COVID-19 Pandemic, Wang and al 2022*) and the poor explicability of the obtained results are still a significant drawback. Importantly, the vast majority of these studies have provided only binary classifications, seeking either to disentangle the diagnosis of COVID-19 from alternative causes of acute respiratory failure or to assist on the identification of isolated LUS patterns (pleural line (13) , lung edema (14)). Furthermore, none of these networks was able to detect all clinically relevant (A, B, C, pleural effusion and pleural thickening) LUS patterns.

Aiming to fill this knowledge gap and lay the foundation needed to develop an end-to-end tool for computer-assisted analysis of COVID-19 patient's LUS data, we followed an original knowledge transfer approach from satellite to medical imaging based on semantic segmentation and signal processing. Semantic segmentation is a form of pixel-level prediction where each pixel in an image is classified according to a category. Thereby, we were able to provide a new automatic voxel-wise classifier, which was able to identify all the clinically relevant LUS patterns that can be observed in this setting (pleural line, lung oedema, lung consolidation, pleural effusion). Last but not least, to increase the explicability, or at least the interpretability of our medical-assist tool, we used these DL methods not as a black box given to the physician, but as a pre-processing step to a signal analysis process that will refine the result of the network.

MATERIALS AND METHODS

STUDY DESIGN

The whole dataset was prospectively collected at the ICUs from both the University Hospital Purpan (Toulouse, France) and Cayenne Hospital (French Guyana, France) between July 2020 and March 2021. Patients were managed by physicians according to current guidelines and recommendations for critically ill COVID-19 patients (15–17) . The study was approved by the ethics committee of the University Hospital of Toulouse, Toulouse, France (*Comité Consultatif pour la Protection des Personnes*, Ref. 2020-A01225-48); written consent was obtained from all participants. COVID-19 diagnoses were confirmed by positive RT-PCR assay for pharyngeal swap specimens.

POPULATION

We prospectively recruited adult COVID-19 patients who were in acute respiratory failure (ARF) at hospital admission. ARF was defined as patient's blood oxygen saturation as measured by pulse oximetry < 90% while breathing room air or respiratory rate > or = 30 breaths / min (18). Exclusion criteria were patient's history of chronic respiratory disease and the lack of LUS image.

LUNG ULTRASOUND EXAMINATION

All patients underwent a LUS assessment by senior critical care practitioners, with advanced level of thoracic ultrasound training (AA, SB, SS). The level of agreement between raters for the LUS findings has been previously reported (19,20). Lung ultrasound assessment was performed with HP Sonos 5500 (Hewlett-Packard Development Company, LP) and Sonosite M-Turbo (Fujifilm Sonosite Inc, WA, USA) 2- to 4- MHz probes. As previously reported, six quadrants were defined for each hemithorax (1,21).

Following international guidelines for LUS study and data reporting (1,2,21), we used consensual semiotics criteria (figure 1) :

- The normal pleural line was defined as a horizontal hyperechoic line visible below the rib line.

- Pleural effusion was defined as a hypoechoic collection limited by the diaphragm and the pleura (PE profile).
- A normal lung pattern was defined as the presence in a quadrant of lung sliding with reverberating horizontal A lines (A profile).
- Alveolar consolidation was defined as the presence of poorly defined heterogenous wedge-shaped hypoechoic images. We distinguished two patterns of alveolar consolidation during COVID-19:
    - Subpleural non-translobar (C1 profile) (22) which might correspond to peripheral lung embolism (23)
    - Posterior translobar with occasional mobile air bronchograms (C2 profile).
- Alveolar-interstitial syndrome was defined as the presence of more than two vertical lines B lines in a given lung region. To specifically address the usefulness of LUS evaluation to provide semi-quantitative pulmonary oedema assessment, we defined three B-lines classes:
    - B1 profile (thin, multiple and well-defined)
    - B2 profile (large and coalescent)
    - B3 profile ("shining white lung") (24) .

DATA ANNOTATIONS

LUS frames were annotated by 3 medical experts (AA, SB, SS) from Critical Care Units of University Hospital of Toulouse (Toulouse, France) and Hospital of Cayenne (French Guyana, France). These raters are all senior critical care practitioners, with advanced level of thoracic ultrasound training. LUS frames from patients affected by COVID-19 with different degree of severity were gathered and labeled using Clickpoints© annotation tool (Figure 2). Ten random frames of each scan are used to ensure all patterns can be seen yet avoiding too much data redundancy. In addition to LUS semiotics labels, we also used as input annotated pleural line, rib, diaphragm, liver and spleen annotated images. It is worth noting that in order to extract all relevant information from our LUS dataset, most of the not noisy frame pixels have been labeled, making it possible for the network and post-processing to get additional features in the analysis.

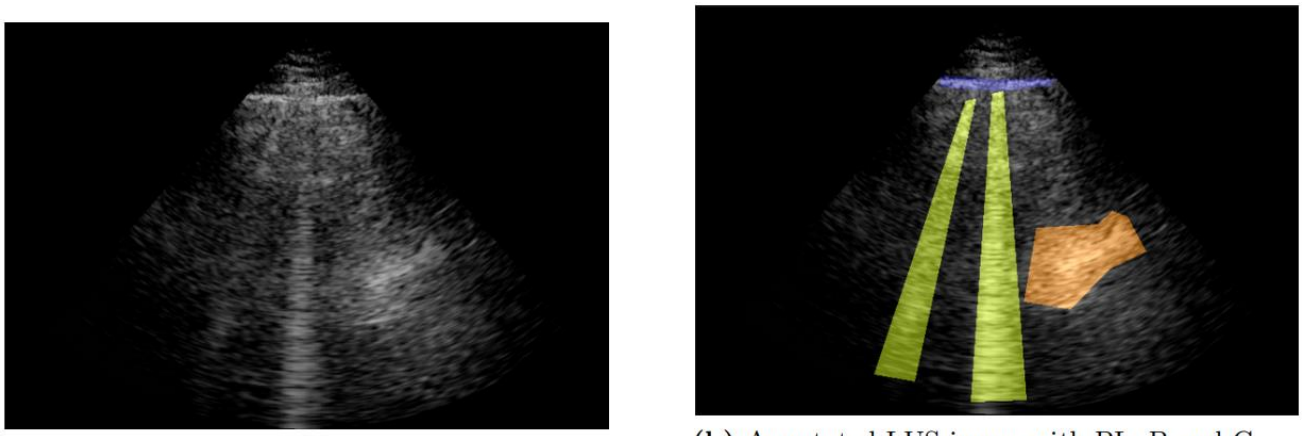

(a) Example of Ground-Truth LUS image

(b) Annotated LUS image with PL, B and C patterns

Fig 2. Labelisation of LUS image

PRE-PROCESSING

In order to lower the bridge between the different ultrasound systems, data augmentation was used. Indeed, artificially increasing LUS images by mixing the contrast, gamma and added blur helped move one image from one ultrasound system modality to another. As some patterns features are close, similar classes were merged into one super-class (e.g., B superclass). In addition, minor classes not helping in the segmentation process were discarded (e.g., spleen). Eventually, the dataset used in the training process is composed of 5 classes: Pleural Line, A pattern, B superclass, C pattern and background.

LUS PATTERNS SEGMENTATION

Semantic segmentation is the process of classifying each pixel of an image. In the current use case, a semantic segmentation neural network is used to emphasize the disease markers (Figure 3). Those markers were present and annotated in the dataset. The function Φ of the network maps an input LUS image X to a multi-class Z image with equal dimensions, so that every pixel of the i class of Z is detected as a class pixel or non-class pixels.

In most semantic segmentation network, Φ is divided in two stages : Φenc learns the features inside the image and Φdec transpose the learned features into a x × y × i Z segmentation output.

Both Φenc and Φdec are composed of convolution and activation layers ψ learned during the training process. As Φenc reduce the dimension as the layer continues, Φdev increase layers dimensions. The final ψm layer of Φdec is a x × y × i matrix where every pixel is assigned to a class probability :

$$\Phi : \underset{x \times y}{\mathcal{X}} \rightarrow \underset{x \times y \times i}{\mathcal{Z}}$$

$$\Phi_{enc} : \underset{x \times y}{\psi_0} \rightarrow \underset{\frac{x}{2} \times \frac{y}{2}}{\psi_1} \ldots \rightarrow \underset{\frac{x}{2^n} \times \frac{y}{2^n}}{\psi_n}, \Phi_{dec} : \underset{\frac{x}{2^n} \times \frac{y}{2^n}}{\psi_n} \ldots \rightarrow \underset{\frac{x}{2} \times \frac{y}{2}}{\psi_{m-1}} \rightarrow \underset{x \times y \times i}{\psi_m}$$

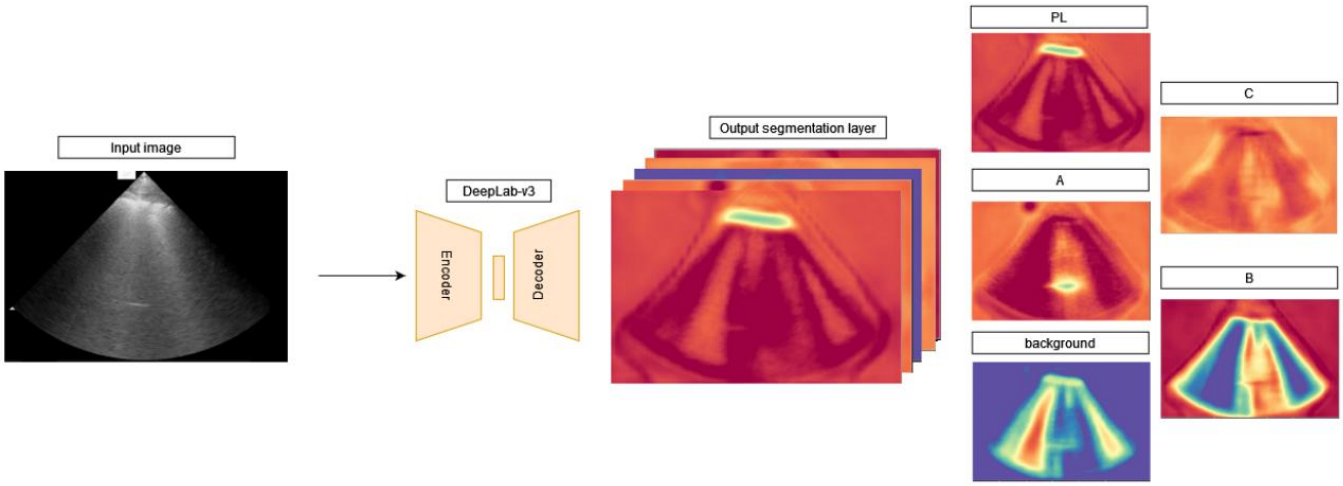

Fig 3. LUS image is segmented in 5 classes : Pleural line, A line, B line, C pattern and background

It is important to pick a correct loss for accurately training the network. Regular training of segmentation network uses the cross-entropy (CE) loss. However, in unbalanced class distribution settings, CE will be biased toward the majority class. In LUS images, most pixel belongs to the background class, training a network with CE will result in blurry frontier between relevant information and background. To counter balance this bias, our network is trained with a composition of two losses, focal loss L_{FL} (25) and boundary loss L_{BL} (26).

$$\mathcal{L}_{FL} = \int_i^C \int_\Omega (1 - s_\theta^i(p))^\gamma g_i(p) \log s_\theta^i(p) dp dc \quad (3)$$

$$\mathcal{L}_{BL} = \int_\Omega \Delta_G(p) s_\theta(p) dp \quad (4)$$

$$\mathcal{L} = \mathcal{L}_{FL} + \alpha \mathcal{L}_{BL} \quad (5)$$

Where sθ is the last layer ψm of Φdec, g is the ground truth, p ⊂ Ω, the set of pixels, ΔG is a function returning −Dp or Dp with Dp being the L2 distance from p to the pattern contour of gi, α is a constant to balance the two losses. As seen in Eq. 3, L_{BL} weights hard to classify example. This is essential for segmenting C-patterns that are rare and have difficult features to learn. L_{BL} adds region-wise distance which is helpful to have strong segmentation boundary, it forces strong gradient from pattern region to background. Several network architectures have been tested: U-Net (27) , DeepLab-v3 (28), LinkNet (29) , MANet (30) and YNet (31) .

METRICS

To assess the performance of the different architectures the F1 metric was chosen. F1 is the harmonic mean of precision and sensitivity. This follows the use of focal and boundary losses. Precision highlights well classified pixels that are not outside of patterns region whereas recall shows if all pixel belonging to patterns are found. For regions where we want near perfect delimitation, such as B, PL and A, precision will be an important metric. C-pattern is harder to classify and the pattern region is uncertain, in this case it is preferred to force the detection, networks showing high recall will be favored.

Additionally, ROC curve (receiver operating characteristic curve) displaying the relation of true positive rate against false positive rate at different classification thresholds, was also computed.

POST PROCESSING

The final layer ψ_m of the semantic segmentation network (Eq. 2) contains the pixel-wise classification for the 5 classes. This view can be directly used as a processed view of a LUS image. However, some information is lacking, it does not give an immediate overview of the lung condition of a patient. Ideally, a post-processing analysis on top of ψ_m would give a counting of B-Lines with their dimensions and a discrimination of the sub-classes of B superclass.

The B superclass was initially composed of 4 classes: B well defined, B large, White lung and Z-Line. Those sub-classes were particularly hard to discriminate one from another. Indeed, drawing the frontier from a B2 to a B3 is difficult as well as classifying a well-defined B-Line not erasing the A-Line as a Z-Line. This analysis may differ depending on the physician view. To tackle this problem (Figure 4), we introduce a post-processing tool based on signal analysis. A LUS image can be seen as a cone starting from an origin point O(x_o,y_o) where the first angle ϑ_0 would be defined by the leftmost line from O to the furthest left point T_l and the final angle ϑ_r would be defined by the rightmost line from O to the furthest right point T_r of the LUS image. {O, T_l, T_r} defines a triangle containing all the angles of the LUS image. From this triangle each line from each angle can be computed using the Bresenham's algorithm (32). For every two points O(x_o,y_o) and P(x_p,y_p) in X , the Bresenham's algorithm (BA) gives a list of pixels L_i crossing the line.

$$BA(\mathcal{X}_{\mathcal{O},\mathcal{T}_l,\mathcal{T}_r}) = L_{l\to t} \qquad (6)$$

The L grid can be mapped directly on ψ_m to retrieve class i signature alongside each ϑ angle.

$$L_\theta(\psi_{m,i}) = \omega_{\theta,i} \qquad (7)$$

$\omega_{\vartheta_l\to\vartheta_r,B}$ will then be the distribution of B pattern around the cone of the LUS image. Pixels not belonging to the B class can be filtered out by applying a simple threshold on the class probability. From $\omega_{\vartheta,B}$ a distribution $\mu_{\vartheta,B}$ of the number of points belonging to the B class on angle ϑ is obtained. The $\mu_{\vartheta_l\to\vartheta_r,B}$ distribution is enhanced with a 1-D Gaussian filter G_B

removing negligible local variations. Δ_{grad} is the gradient linked to the $G_B(\vartheta)$ function.

$$G_B(\theta) = \frac{1}{\sqrt{2\pi}\sigma} e^{\frac{\mu_{\theta,B}^2}{2\sigma^2}}, \Delta_{grad,B}(\theta) = \frac{\delta G_B(\theta)}{\delta\theta} \quad (8)$$

From GB(θ) and Δgrad,B(θ), local maxima are picked, they are the sources of B-Lines. By walking on the gradient and comparing Δgrad,B(θsource) with Δgrad,B(θθsource → θl) and Δgrad,B(θθsource → θr), the B-Line dimension can be found. If the gradient is inverted, then another B-Line is starting, if the gradient is flattened, this marks a limit of the current B-Line.

With B-Line source θsource and dimensions {θlb,θrb}, the B-Line subclass can be discriminated. A White Lung would not find neighbors during the Δgrad,B(θθsource → θl) and Δgrad,B(θθsource → θr) walks. B-Lines θsource stopped crossing A-Lines determined by ψm,A will be detected as Z-Line. Alternatively, θsource starting while ψm,PL could not see PL could be a sign of C-pattern that can be consolidated by ψm,C.

(a) Input image

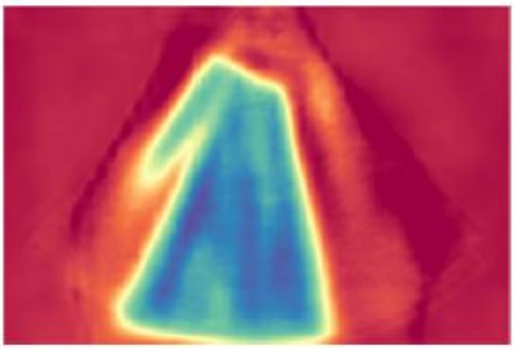

(c) $\psi_{m,B}$

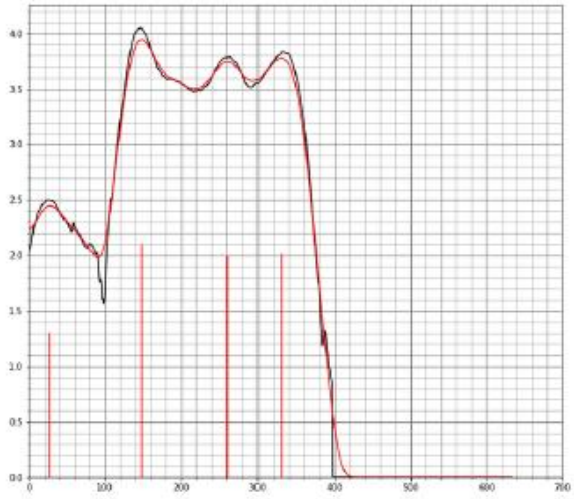

(b) Signal analysis, in black : $\mu_{\theta_l \to \theta_r, B}$, in red $G_B(\theta_l \to \theta_r)$ and peaks

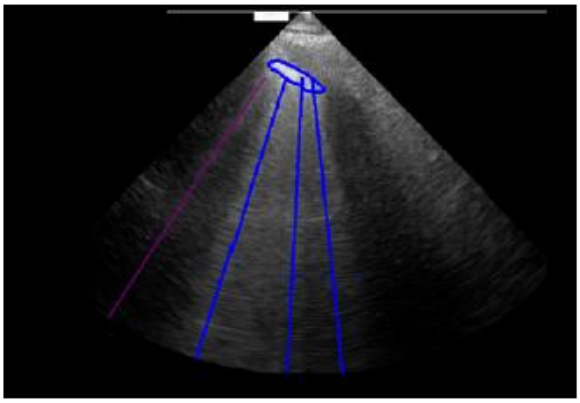

(d) Output, Z-Line in purple - B-Line in blue

Fig 4. Post processing analysis : (a) input image is processed with B-line highlighting (c), (b) is the B signature around the LUS image cone, (d) is the view with B-line subclass identification.

EXPLAINABILITY

We used the Gradient-weighted Class Activation Mapping (Grad-CAM) method to visually explain the model's predictions (33) . Grad-CAM involves visualizing the gradients of the prediction of a particular image with respect to the activation of the final convolutional layer of the CNN. A heatmap is produced that highlights the area of the input image that were most contributory to the model's classification decision.

RESULTS

ULTRASOUND DATA

Overall, 5000 LUS frames from 58 patients affected by COVID-19 (Table 1 and 2) with different degree of severity were gathered and labeled. Data analysis was conducted on CNES (French National Center of Space Studies) HPC platform, namely on NVIDIA A100 and V100 cards. The total amount of frames was divided 5-fold: 4 folds were used for the training and the last one for validation. The validation fold was created in a fair representation of each pattern. The visual results were conducted using an independent fold on frames which was not initially annotated by the physicians (Table 3).

Labelled Elements	
Number of patients	58
Number of scans	510
Number of labelled frames	5 000

Table 1. Labelled elements of our LUS dataset

Annotation pattern summary	
Pleural Line	4214
B-line large	2627
A-line	1397
B-line well defined	755
C-pattern	621
No pattern	586
White Lung	367
Z-line	308
Air Bronchogram	235
Pleural Effusion	228
Rib	176
Diaphragm	103
Spleen	8
Liver	2
Total Annotations	11 627

Table 2. Annotation pattern summary of our LUS dataset

Train	Validation	Test
52/433/4330	5/44/440	17/204/2040

Table 3. Division of sets (patients /scans / frames)

SEGMENTATION ACCURACY

Table 4 shows the architecture of the results during the segmentation task. When Networks are close one to another, DeepLab showed better result on recall of different patterns and so was chosen as standard segmentation model for the signal analysis. The ROC curve in Figure 5 was computed using the DeepLab segmentation model.

Network	F1	Recall	Precision
MANet	0.9662	0.9665	**0.9669**
LinkNet	0,9656	0.9656	0.9661
DeepLab	**0.9663**	**0.9666**	0.9662
YNet	0.9618	0.9594	0.9649

Table 4. Segmentation result

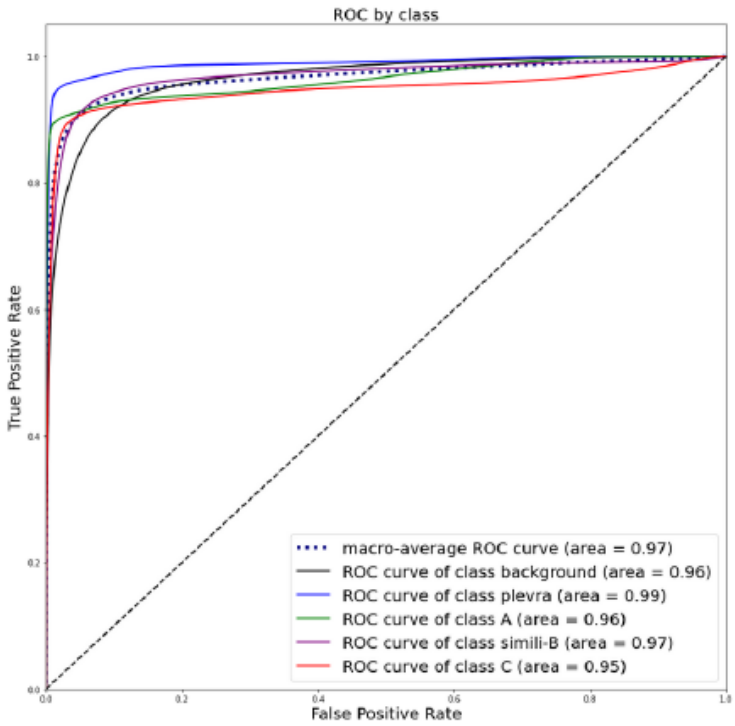

Fig 5. ROC curve on different patterns

It is worth noting (Figure 6), if PL was almost perfectly segmented, alternatives patterns such as B and C were harder to segment. We suggest that this result might be related to the fact that PL features (position, shape) are close for every frame whereas other patterns are based on more heterogenous ultrasonographic signs. In addition, C-pattern frontier was semantically hard to estimate, probably because this result in the network being sometimes too greedy or restrictive compared to the clinician label.

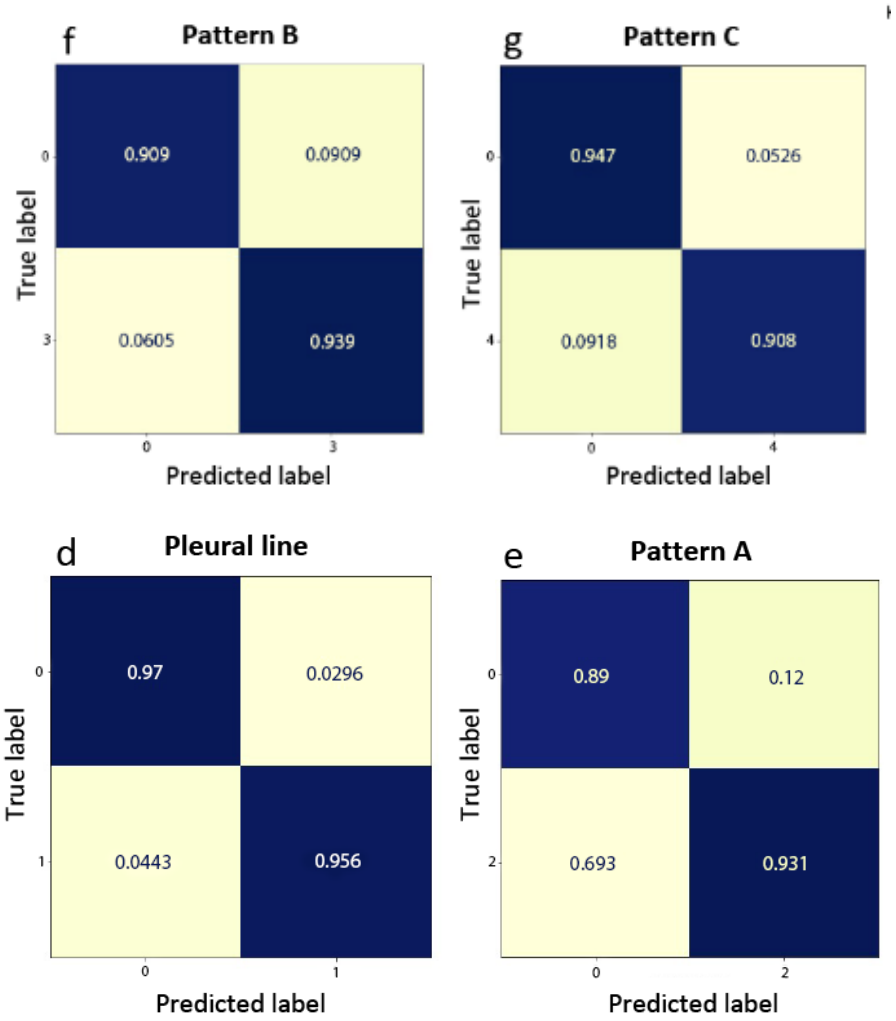

Fig 6. Confusion matrix of each class after sigmoid and threshold

EXPLAINABILITY OF RESULTS

If the segmentation metrics gives relevant information on the validation set, estimating the perceptual quality of the post-processing analysis on the unlabeled test set cannot be done with metrics. The Grad-CAM Explainability algorithm was applied to the model and results are conveyed by color on the heatmap, overlaid on the input images.

Hence, as Figure 7 shows, the physician in charge of the patient, might be given a multi-view panel, encompassing images from the input to the post-processing output with both ψm,B and ψm,C that highlights relevant pixels. The key activation areas for all classes included the pleural line and the main axis of B lines (B pattern).

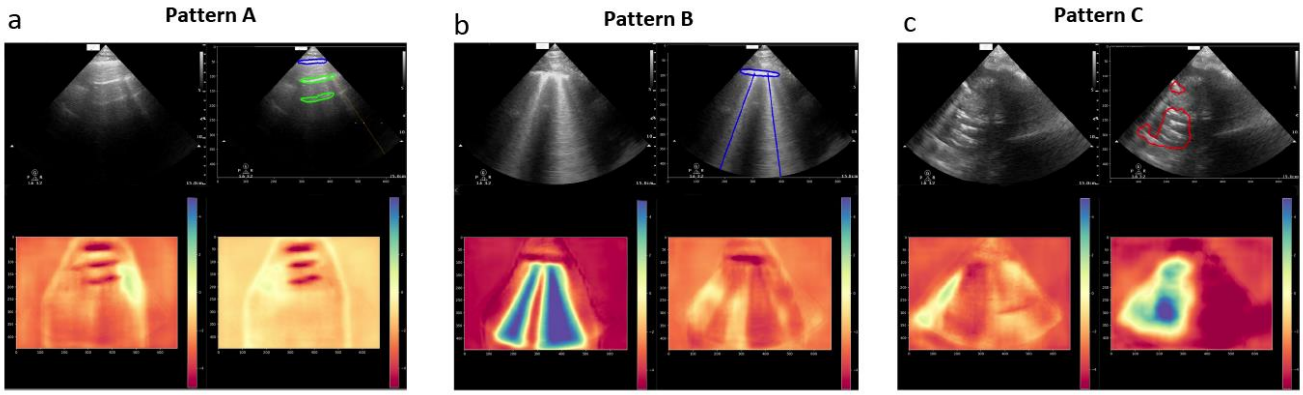

Fig 7. Results on unlabeled set

EXTERNAL VALIDATION

The current semantic segmentation network was eventually tested on the POCUS dataset (34) from another cohort. Interestingly, nonetheless significant differences between both LUS dataset, including acquisition modalities and image dimension, our semantic segmentation network seemed to accurately identity A, B and C LUS patterns (Figure 8).

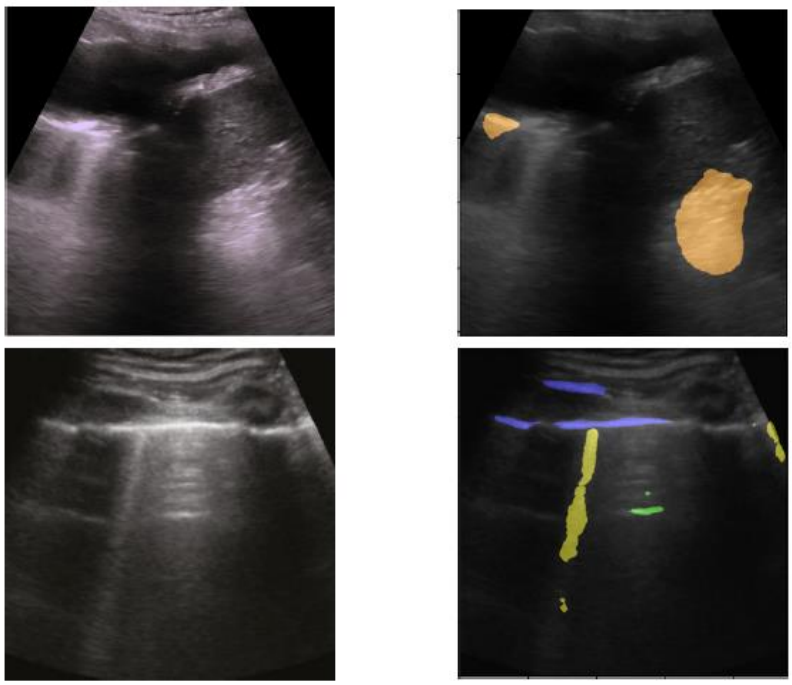

Fig 8. Results on POCUS dataset : PL in blue, A in green, B in yellow, C pattern in orange

DISCUSSION

In this study, an original semantic segmentation and signal processing model was successfully trained to identify clinically meaningful LUS patterns from a COVID-19 patient's dataset. The model was able to accurately identify at a frame-based level, voxel-wise signatures of normal lung (A pattern), lung edema (B pattern) or loss of aeration (C pattern) and pleural effusion (PE pattern). Our results, within the context of the limitations outlined below, are the first of their kind to provide an end-to-end explainable digital tool, which is able to accurately distinguish between all these canonical LUS patterns.

As a variant with previous studies in this field, which were designed to automatically classify specific and isolated LUS patterns *(Supplementary table S1,* (5) our study sought to provide whole-frame and pixel-level sonographic LUS images segmentation. Consequently, we developed and validated a new numerical solution allowing the automatized detection of all LUS canonical patterns that are currently observed in COVID-19 patients. The performance of this tool was assessed using data augmentation and a batch of 1/3 of our data that was held back from the training process, thereby estimating generalized performance and defending against model overfitting that may otherwise exaggerate Deep Learning results.

Explainability efforts using Grad-CAM methods were employed to allow insight into the regions of LUS images that contributed most to the prediction of the neural network. Indeed, the information given by the final layer of the network is rich and can be used directly by a clinician as a processed view of the LUS image or by any post-processing analysis. Interestingly, although the exact mechanism of distinction is unknown, the Grad-CAM heatmap results suggest the model follows pattern recognition similar to those applied by medical experts (33) . Indeed, the most active images areas in driving model's performances are centered around the pleural line and the B-lines axis.

It is worth noting that our model was built upon a rather homogenous prospective dataset of 5000 frames, which is one the largest volume of LUS data from COVID-19 patients reported to date. Owing to the scarcity of labelled LUS data, these volume and homogeneity,

both in terms of LUS acquisition settings and the implication of a reduced number of medical assessors with reported good inter-observed variability, does compare favorably to other published LUS works (5,19,20).

Our study also have limitations inherent to the opaqueness that is intrinsic to Deep Learning methods. Despite using Grad-CAM and selectively mastering few physical properties of the images, the decision made by our model are not fully explained and we are unable to critique its methods. Moreover, our data were all from severely ill hospitalized patients and our results may not generalize to those who are less ill. Finally, despite the fact that our study used one of the largest and more homogeneous LUS datasets from COVID-19 patients to date, this amount of data is small when compared to alternative AI-based computer science studies and the addition of further training data could have aided with generalizability of the model.

CONCLUSION

The analysis of LUS images for the diagnosis of COVID-19 is challenging and need to be tackle from an explainable and medical view. In this paper we propose a new and accurate end-to-end tool with Deep Learning used not as a “black box” given to the clinician, but as a pre-processing step to a signal analysis process that will refine the result of the network. We think that giving a complete view of both neural network output and final decision to the clinician seems to be a good way to build trustworthy results. Overall, our work opens the door toward plausible early, automated COVID-19 severity scoring and patient’s follow-up. The eventual integration of this model into ultrasound hardware seems plausible as a method to achieve real-time, point-of-care and patient’s bedside diagnosis and prognosis of COVID-19 or other specific respiratory illness that increasingly claimed attention for the computer-assisted analysis of LUS data.

Vu et permis d'imprimer
Par délégation, la Vice-Doyenne de la Faculté de Santé
Directrice du Département Médecine Maïeutique Paramédical

Professeure Odile RAUZY

Pr. Stein SILVA SIFONTES
Médecine Intensive Réanimation N° RPPS - 10001536648
Réanimation Polyvalente - Surveillance Continue et Déchocage
Bâtiment URM (Urgences-Réanimation-Médecines)
TSA 40031 - 31059 TOULOUSE CEDEX 9
Tél. : 05.61.77.22.61

REFERENCES

1. Mojoli F, Bouhemad B, Mongodi S, Lichtenstein D. Lung Ultrasound for Critically Ill Patients. Am J Respir Crit Care Med. 15 mars 2019;199(6):701-14.

2. Lichtenstein DA, Mezière GA. Relevance of lung ultrasound in the diagnosis of acute respiratory failure: the BLUE protocol. Chest. juill 2008;134(1):117-25.

3. Peng QY, Wang XT, Zhang LN, Chinese Critical Care Ultrasound Study Group (CCUSG). Findings of lung ultrasonography of novel corona virus pneumonia during the 2019-2020 epidemic. Intensive Care Med. mai 2020;46(5):849-50.

4. Volpicelli G, Gargani L, Perlini S, Spinelli S, Barbieri G, Lanotte A, et al. Lung ultrasound for the early diagnosis of COVID-19 pneumonia: an international multicenter study. Intensive Care Med. avr 2021;47(4):444-54.

5. Wang J, Yang X, Zhou B, Sohn JJ, Zhou J, Jacob JT, et al. Review of Machine Learning in Lung Ultrasound in COVID-19 Pandemic. J Imaging. 5 mars 2022;8(3):65.

6. Aguersif A, Sarton B, Bouharaoua S, Gaillard L, Standarovski D, Faucoz O, et al. Lung Ultrasound to Assist ICU Admission Decision-Making Process of COVID-19 Patients With Acute Respiratory Failure. Crit Care Explor. juin 2022;4(6):e0719.

7. Poggiali E, Dacrema A, Bastoni D, Tinelli V, Demichele E, Mateo Ramos P, et al. Can Lung US Help Critical Care Clinicians in the Early Diagnosis of Novel Coronavirus (COVID-19) Pneumonia? Radiology. juin 2020;295(3):E6.

8. Chavez MA, Shams N, Ellington LE, Naithani N, Gilman RH, Steinhoff MC, et al. Lung ultrasound for the diagnosis of pneumonia in adults: a systematic review and meta-analysis. Respir Res. déc 2014;15(1):50.

9. Chassagnon G, Vakalopoulou M, Paragios N, Revel MP. Artificial intelligence applications for thoracic imaging. Eur J Radiol. févr 2020;123:108774.

10. Shan F, Gao Y, Wang J, Shi W, Shi N, Han M, et al. Abnormal lung quantification in chest CT images of COVID-19 patients with deep learning and its application to severity prediction. Med Phys. avr 2021;48(4):1633-45.

11. Zhou T, Canu S, Ruan S. An automatic COVID-19 CT segmentation network using spatial and channel attention mechanism. Int J Imaging Syst Technol. mars 2021;31(1):16-27.

12. Wang S, Zha Y, Li W, Wu Q, Li X, Niu M, et al. A fully automatic deep learning system for COVID-19 diagnostic and prognostic analysis. Eur Respir J. août 2020;56(2):2000775.

13. Carrer L, Donini E, Marinelli D, Zanetti M, Mento F, Torri E, et al. Automatic Pleural Line Extraction and COVID-19 Scoring From Lung Ultrasound Data. IEEE Trans Ultrason Ferroelectr Freq Control. nov 2020;67(11):2207-17.

14. Baloescu C, Toporek G, Kim S, McNamara K, Liu R, Shaw MM, et al. Automated Lung Ultrasound B-Line Assessment Using a Deep Learning Algorithm. IEEE Trans Ultrason Ferroelectr Freq Control. nov 2020;67(11):2312-20.

15. Poston JT, Patel BK, Davis AM. Management of Critically Ill Adults With COVID-19. JAMA [Internet]. 26 mars 2020 [cité 27 août 2022]; Disponible sur: https://jamanetwork.com/journals/jama/fullarticle/2763879

16. Adalja AA, Toner E, Inglesby TV. Priorities for the US Health Community Responding to COVID-19. JAMA. 14 avr 2020;323(14):1343.

17. Phua J, Weng L, Ling L, Egi M, Lim CM, Divatia JV, et al. Intensive care management of coronavirus disease 2019 (COVID-19): challenges and recommendations. Lancet Respir Med. mai 2020;8(5):506-17.

18. Fan E, Del Sorbo L, Goligher EC, Hodgson CL, Munshi L, Walkey AJ, et al. An Official American Thoracic Society/European Society of Intensive Care Medicine/Society of Critical Care Medicine Clinical Practice Guideline: Mechanical Ventilation in Adult Patients with Acute Respiratory Distress Syndrome. Am J Respir Crit Care Med. 1 mai 2017;195(9):1253-63.

19. Bataille B, Riu B, Ferre F, Moussot PE, Mari A, Brunel E, et al. Integrated use of bedside lung ultrasound and echocardiography in acute respiratory failure: a prospective observational study in ICU. Chest. déc 2014;146(6):1586-93.

20. Silva S, Biendel C, Ruiz J, Olivier M, Bataille B, Geeraerts T, et al. Usefulness of cardiothoracic chest ultrasound in the management of acute respiratory failure in critical care practice. Chest. sept 2013;144(3):859-65.

21. Volpicelli G, Elbarbary M, Blaivas M, Lichtenstein DA, Mathis G, Kirkpatrick AW, et al. International evidence-based recommendations for point-of-care lung ultrasound. Intensive Care Med. avr 2012;38(4):577-91.

22. Soldati G, Smargiassi A, Inchingolo R, Buonsenso D, Perrone T, Briganti DF, et al. Is There a Role for Lung Ultrasound During the COVID-19 Pandemic? J Ultrasound Med Off J Am Inst Ultrasound Med. juill 2020;39(7):1459-62.

23. Zotzmann V, Lang CN, Bamberg F, Bode C, Staudacher DL. Are subpleural consolidations indicators for segmental pulmonary embolism in COVID-19? Intensive Care Med. juin 2020;46(6):1109-10.

24. Volpicelli G, Lamorte A, Villén T. What's new in lung ultrasound during the COVID-19 pandemic. Intensive Care Med. juill 2020;46(7):1445-8.

25. Lin TY, Goyal P, Girshick R, He K, Dollar P. Focal Loss for Dense Object Detection. In: 2017 IEEE International Conference on Computer Vision (ICCV) [Internet]. Venice: IEEE; 2017 [cité 14 juill 2022]. p. 2999-3007. Disponible sur: http://ieeexplore.ieee.org/document/8237586/

26. Kervadec H, Bouchtiba J, Desrosiers C, Granger E, Dolz J, Ben Ayed I. Boundary loss for highly unbalanced segmentation. Med Image Anal. janv 2021;67:101851.

27. Ronneberger O, Fischer P, Brox T. U-Net: Convolutional Networks for Biomedical Image Segmentation. In: Navab N, Hornegger J, Wells WM, Frangi AF, éditeurs. Medical Image Computing and Computer-Assisted Intervention – MICCAI 2015 [Internet]. Cham: Springer International Publishing; 2015 [cité 14 juill 2022]. p. 234-41. (Lecture Notes in Computer Science; vol. 9351). Disponible sur: http://link.springer.com/10.1007/978-3-319-24574-4_28

28. Chen LC, Papandreou G, Schroff F, Adam H. Rethinking Atrous Convolution for Semantic Image Segmentation. ArXiv170605587 Cs [Internet]. 5 déc 2017 [cité 14 juill 2022]; Disponible sur: http://arxiv.org/abs/1706.05587

29. Chaurasia A, Culurciello E. LinkNet: Exploiting Encoder Representations for Efficient Semantic Segmentation. 2017 IEEE Vis Commun Image Process VCIP. déc 2017;1-4.

30. Xu Y, Lam HK, Jia G. MANet: A two-stage deep learning method for classification of COVID-19 from Chest X-ray images. Neurocomputing. 5 juill 2021;443:96-105.

31. Lan H, Jiang D, Yang C, Gao F, Gao F. Y-Net: Hybrid deep learning image reconstruction for photoacoustic tomography in vivo. Photoacoustics. déc 2020;20:100197.

32. Bresenham JE. Algorithm for computer control of a digital plotter. IBM Syst J. 1965;4(1):25-30.

33. Selvaraju RR, Cogswell M, Das A, Vedantam R, Parikh D, Batra D. Grad-CAM: Visual Explanations from Deep Networks via Gradient-based Localization. Int J Comput Vis. févr 2020;128(2):336-59.

34. Born J, Brändle G, Cossio M, Disdier M, Goulet J, Roulin J, et al. POCOVID-Net: Automatic Detection of COVID-19 From a New Lung Ultrasound Imaging Dataset (POCUS) [Internet]. arXiv; 2021 [cité 27 août 2022]. Disponible sur: http://arxiv.org/abs/2004.12084

SUPPLEMENTARY MATERIAL

Table S1 : Summary of research articles on AI applications of LUS for COVID-19. (5)

Articles	Time	Datasets	Techniques	Main Tasks	Results
Born et al. [59]	May 2020	POCUS dataset [59]: 64 videos (39 COVID-19, 14 bacterial pneumonia, and 11 healthy controls)	VGG16	Classifying frames/videos as COVID-19, bacterial pneumonia, or healthy.	* AUC: 0.94 Accuracy: 0.89 Sensitivity: 0.96 Specificity: 0.79 F1-score: 0.92
Roy et al. [62]	August 2020	35 patients (17 COVID-19, 4 COVID-19 suspected, and 14 healthy controls)	Spatial Transformer Networks (STN) & U-Net	Scoring frames/videos; Segmenting COVID-19 imaging biomarkers.	Accuracy: 0.96 Recall: 0.6 ± 0.07 Precision: 0.7 ± 0.19 F1-score: 0.61 ± 0.12
Horry et al. [102]	August 2020	Multimodal dataset of X-ray, ultrasound, and CT (COVID-19, pneumonia, and Normal)	VGG16/19, ResNet50, Inception V3, Xception, InceptionResNetV2, NASNet, and DenseNet121	Classifying COVID-19, pneumonia, and normal cases with limited datasets.	Recall: 1.0 Precision: 1.0 F1-score: 1.0
Born et al. [60]	September 2020	139 recordings (63 COVID-19, 41 non-COVID-19 pneumonia, and 35 healthy controls)	VGG16	Classifying COVID-19 US videos; Localizing spatio-temporally pulmonary biomarkers.	AUC: 0.94 ± 0.03 Recall: 0.98 ± 0.04 Specificity: 0.91 ± 0.08 Precision: 0.91 ± 0.08 MCC: 0.89 ± 0.06 F1-score 0.94 ± 0.04
Hou et al. [86]	October 2020	2800 images (740 A-line, 1150 B-line and 910 consolidation images)	Adjusted Bias (Saab) multilayer network	Classifying consolidation vs A-line vs B-line.	Accuracy: 0.97
Roberts et al. [74]	November 2020	POCUS dataset [59]	VGG16 & ResNet18	Classifying COVID-19, bacterial pneumonia, and control cases.	Accuracy: 0.86 AUC: 0.90
Carrer et al. [66]	November 2020	Subsets of the *ICLUS-DB* database [66]: 29 cases (10 negatives, 15 positives, and four suspected COVID-19)	SVM	Detecting pleural line automatically; Scoring LUS images.	Accuracy: 0.85–0.98 Sensitivity: 0.85–0.93 Specificity: 0.95–0.99
Liu et al. [95]	November 2020	71 patients with 6836 images sampled from 678 videos	ResNet50	Classifying A-line, B-line, pleural lesion, and pleural effusion.	Accuracy: 0.98 Sensitivity: 0.99 Specificity: 0.92
Baloescu et al. [93]	November 2020	2415 subclips rated for severity of B-lines, from 0 (none) to 4 (severe)	Custom-designed CNNs	Detecting B-lines from LUS clips to evaluate COVID-19 severity.	AUC: 0.97 Sensitivity: 0.81–0.98 Specificity: 0.84–0.99 Kappa: 0.79–0.97
Che et al. [90]	February 2021	POCUS dataset and ICLUS-DB: 51 COVID-19, 13 pneumonia, and 12 healthy subjects	ResNet	Classifying COVID-19 from LUS data.	Accuracy: 0.95 Recall: 0.99 Precision: 0.96 F1-score: 0.9
Muhammad et al. [89]	February 2021	121 videos (45 for COVID-19, 23 for bacterial pneumonia, and 53 for healthy); 40 images (18 for COVID-19, 7 for bacterial pneumonia, and 15 for healthy)	ResF module	Classifying COVID-19, bacterial pneumonia, and healthy cases.	AUC: 0.99 Accuracy: 0.92 Recall: 0.93 Precision: 0.92
Dastider et al. [88]	February 2021	ICLUS-DB: 58 videos (38 with a convex probe, and 20 with a linear probe) scored based on a 4-level scoring system	DenseNet-201	Scoring LUS images.	Accuracy: 0.79 ± 0.06/0.68 ± 0.03 Sensitivity: 0.79 ± 0.06/0.68 ± 0.03 Specificity: 0.90 ± 0.03/0.77 ± 0.14 F1-score: 0.79 ± 0.06/0.67 ± 0.03
Arntfield et al. [97]	February 2021	243 patients (81 hydrostatic pulmonary edema (HPE), 78 non-COVID ARDS (NCOVID), and 84 COVID-19)	Xception	Classifying COVID-19, NCOVID and HPE pathologies.	AUC: 0.97 Sensitivity: 0.92 Specificity: 0.88 Precision: 0.71 F1-score 0.81
Tsai et al. [77]	March 2021	70 patients (39 abnormal and 31 normal)	STN	Classifying normal vs pleural effusion classes.	Accuracy: 0.92 Recall: 0.88 F1-score: 0.9
Hu et al. [100]	March 2021	Multicenter and multimodal ultrasound data from 104 patients	ResNeXt	Scoring lung sonograms based on classifications of pathology indicators.	Accuracy: 0.94 Sensitivity: 0.76 Specificity: 0.96 Precision: 0.82

Table S1 (continued)

Articles	Time	Datasets	Techniques	Main Tasks	Results
Xue et al. [98]	April 2021	313 patients classified into four types (mild, moderate, severe, and critical severe)	VGG	Classifying severity of COVID-19 patients from LUS and clinical information.	Accuracy: 0.88 Recall: 0.85 Precision: 0.8 F1-score: 0.87
Gare et at. [84]	April 2021	Four patients (three COVID-19 positives and one control)	U-net	Segmenting A-line, B-line, and pleural line; Classifying normal vs. pneumonia vs. COVID-19.	Accuracy: 0.85 Recall: 0.91 Precision: 0.89 F1-score: 0.90
Mento et al. [78]	May 2021	1488 videos from 82 patients, scored 0-3 scales	STN & U-Net and DeepLab v3+	Scoring LUS videos.	Accuracy: 0.86
Yaron et al. [76]	June 2021	35 patients (17 COVID-19, 4 COVID-19 suspected, and 14 healthy controls)	Resnet18	Scoring LUS frames.	F1-score: 0.69
Raghavi et al. [71]	June 2021	765 images (266 positive COVID-19 and 499 negative cases)	ANN	Classifying a LUS dataset.	Accuracy: 0.84
Awasthi et al. [85]	June 2021	*POCUS* dataset: 64 videos (11 healthy, 14 pneumonia, and 39 COVID-19 patient)	MobileNet	Classifying COVID-19, bacterial pneumonia, and healthy cases.	Accuracy: 0.83 Sensitivity: 0.92 Specificity: 0.71 Precision: 0.83 F1-score: 0.87
Zheng et al. [99]	June 2021	Multimodal dataset: 1393 doctor–patient dialogues and 3706 images for COVID-19 patients; and 607 dialogues and 10,754 images for non-COVID-19 patients	Temporal NN	Classifying COVID-19 vs. non-COVID-19 casese.	Accuracy: 0.98 Sensitivity: 0.99 Specificity: 0.99 Precision: 0.99 AUC: 0.99 F1-score: 0.99
Sadik et al. [91]	July 2021	POCUS dataset [59]	DenseNet-201, ResNet-152V2, Xception, VGG19, and ImageNet	Classifying COVID-19, pneumonia, and normal cases.	Accuracy: 0.91 Sensitivity: 0.91 Specificity: 0.90 F1-score: 0.90
Barros et al. [87]	August 2021	185 videos (69 COVID-19, 50 bacterial pneumonia, and 66 healthy controls)	POCOVID-Net, DenseNet, ResNet, Xception, and NASNet	Classifying COVID-19, pneumonia, and normal cases.	Accuracy: 0.91–0.93 Recall: 0.84-0.97 Specificity: 0.90–1.0 Precision: 0.89–1.0 F1-score: 0.86–0.95
Diaz-Escobar et al. [73]	August 2021	3326 images (1283 for COVID-19, 731 for bacterial pneumonia, and 1312 for healthy controls)	VGG19, InceptionV3, Xception, and ResNet50	Classifying COVID-19, pneumonia, and normal cases.	AUC: 0.97 $\pm$ 0.01 Accuracy: 0.89 $\pm$ 0.02 Recall: 0.86 $\pm$ 0.03 F1-score: 0.88 $\pm$ 0.03 Precision: 0.9 $\pm$ 0.03
Ebadi et al. [81]	August 2021	300 patients (100 for each ARDS feature: A-line, B-line, and consolidation)	3D ConvNet	Classifying A-line, B-line, and consolidation and/or pleural effusion from videos.	AUC: 0.91–0.96 Accuracy: 0.9 Recall: 0.86–0.92 Precision: 0.93–0.98 F1-score: 0.87–0.94
La Salvia et al. [105]	August 2021	450 patients (278 positive and 172 negative cases)	ResNet18, ResNet50	Classifying four/seven classes of LUS.	AUC: 0.98–1.0 Accuracy: 0.98–1.0 Recall: 0.97–0.99 Precision: 0.98–0.99 F1-score: 0.97–0.99
Panicker et al. [94]	September 2021	5000 images from seven subjects (1000 images per class)	VGG16	Detecting pleura and generating acoustic features; Classifying five classes of LUS images.	Accuracy: 0.97 Sensitivity: 0.92 Specificity: 0.98
Mento et al. [79]	September 2021	100 patients with 133 LUS exams scored to four levels	STN & U-Net and DeepLab v3+	Scoring LUS videos.	Accuracy: 0.82
Al-Jumaili et al. [70]	October 2021	2995 images (988 COVID-19, 731 pneumonia, and 1276 regular images, available on Kaggle)	SVM & Resnet18, Resnet50, GoogleNet, and NASNet-Mobile	Detecting pathology features from LUS images; Classifying COVID-19, pneumonia, and regular cases.	Accuracy: 0.99 Sensitivity: 0.99 Specificity: 0.99 F1-score: 0.99

Table S1 (continued)

Articles	Time	Datasets	Techniques	Main Tasks	Results
Karnes et al. [104]	October 2021	13103 normal, 4900 pneumonia, and 8633 COVID-19 frames	LDA & MobileNet	Classifying COVID-19, pneumonia, and healthy cases.	AUC: 0.95
Demi et al. [80]	December 2021	220 patients (100 positive patients and 120 post-COVID-19 patients)	STN & U-Net	Testing protocols for grading LUS.	Accuracy: 0.80
Roshankhah et al. [82]	Decemberc 2021	32 patients (14 confirmed COVID-19, 4 suspected cases and 14 controls)	U-Net	Scoring severity in 4-scale stages; Investigating the impact of various training/test splitting schemes.	Accuracy: 0.95/0.75
Wang et al. [69]	January 2022	27 cases (13 moderate, seven severe, and seven critical cases of COVID-19)	SVM	Scoring the severity of COVID-19 pneumonia by pleural line and B-lines.	AUC: 0.88–1.0 Sensitivity: 0.93 Specificity: 1.0
Durrani et al. [83]	July 2022	28 patients (10 unhealthy and 18 healthy)	STN & U-Net	Detecting Consolidation/Collapse in LUS videos/frames.	AUC: 0.73 ± 0.3 Accuracy: 0.89 ± 0.16 Recall: 0.84 ± 0.23 Precision: 0.59 ± 0.28 F1-score: 0.67 ± 0.25

* Area under curve (AUC).

UNIVERSITÉ TOULOUSE III PAUL SABATIER
Université de Toulouse
FACULTÉ DE MÉDECINE PURPAN

Serment d'Hippocrate

«Au moment d'être admis(e) à exercer la médecine, je promets et je jure d'être fidèle aux lois de l'honneur et de la probité.

Mon premier souci sera de rétablir, de préserver ou de promouvoir la santé dans tous ses éléments, physiques et mentaux, individuels et sociaux.

Je respecterai toutes les personnes, leur autonomie et leur volonté, sans aucune discrimination selon leur état ou leurs convictions. J'interviendrai pour les protéger si elles sont affaiblies, vulnérables ou menacées dans leur intégrité ou leur dignité. Même sous la contrainte, je ne ferai pas usage de mes connaissances contre les lois de l'humanité.

J'informerai les patients des décisions envisagées, de leur raisons et de leurs conséquences.

Je ne tromperai jamais leur confiance et n'exploiterai pas le pouvoir hérité des circonstances pour forcer les consciences.

Je donnerai mes soins à l'indigent et à quiconque me les demandera. Je ne me laisserai pas influencer par la soif du gain ou la recherche de la gloire.

Admis(e) dans l'intimité des personnes, je tairai les secrets qui me seront confiés. Reçu(e) à l'intérieur des maisons, je respecterai les secrets des foyers et ma conduite ne servira pas à corrompre les mœurs.

Je ferai tout pour soulager les souffrances. Je ne prolongerai pas abusivement les agonies. Je ne provoquerai jamais la mort délibérément.

Je préserverai l'indépendance nécessaire à l'accomplissement de ma mission. Je n'entreprendrai rien qui dépasse mes compétences. Je les entretiendrai et les perfectionnerai pour assurer au mieux les services qui me seront demandés.

J'apporterai mon aide à mes confrères ainsi qu'à leurs familles dans l'adversité.

Que les hommes et mes confrères m'accordent leur estime
si je suis fidèle à mes promesses ; que je sois déshonoré(e) et méprisé(e) si j'y manque.»

BIQUET Emma 2022 TOU3 1583

Evaluation d'une méthode de segmentation sémantique pour traiter les images d'échographie pleuropulmonaire de patients Covid19

Contexte : Pandémie à Covid 19 ; difficulté d'accessibilité au scanner des patients intubés les plus graves ; développement de l'intelligence artificielle en médecine avec des résultats prometteurs.
Objectifs : Développer un outil grâce à l'intelligence artificielle capable d'identifier les patterns retrouvés dans la pneumopathie à Covid 19 sur une échographie pleuropulmonaire.
Méthodes : Etude prospective effectuée au CHU de Toulouse et à l'hôpital de Cayenne incluant 58 patients entre juin 2020 et mars 2021 ayant une PCR Covid positive et présentant une insuffisance respiratoire aigüe. Tous les patients inclus ont eu une échographie pleuropulmonaire par un praticien expérimenté. Les images ont été analysés par ces mêmes praticiens, les éléments d'intérêt ont été contourés et labellisés en 5 classes : plèvre ; ligne A ; lignes B ; lignes C et le background. Ces données ont été traitées avec une méthode informatique de segmentation sémantique créant un réseau de neurones à convolution.
Résultats : Au total, 5 000 éléments ont été contourés et labellisés à partir des échographies de 58 patients. Ces 5 000 éléments ont été divisés en 5 sous-groupes dont 4 pour entrainer et tester le réseau neural et 1 pour valider le système. Le réseau neural DeepLab semblerai être le meilleur modèle de segmentation en Recall (sensibilité) et F1. La courbe ROC qui émane du sous-groupe validation retrouve une AUC à 0,96 pour la ligne A ; 0,97 pour les lignes B ; 0,95 pour le profil C.
Conclusion : Le réseau neural DeepLab de segmentation sémantique entrainé permet d'identifier les différentes anomalies sur une échographie pleuropulmonaire de patient présentant une pneumopathie à Covid-19 avec une sensibilité et spécificité proche de 100%.

TITRE EN ANGLAIS : Lung ultrasound pixel-level computer-assisted analysis for Covid 19 Patient

DISCIPLINE ADMINISTRATIVE : Médecine spécialisée clinique

MOTS-CLÉS : Lung ultrasound ; Covid 19 ; deep learning ; semantic segmentation ; neural convolution network

INTITULÉ ET ADRESSE DE L'UFR OU DU LABORATOIRE :
Université Toulouse III-Paul Sabatier
Faculté de médecine Toulouse-Purpan,
37 Allées Jules Guesde 31000 Toulouse

Directeur de thèse : Amazigh AGUERSIF